Int J Earth Sci (Geol Rundsch)
DOI 10.1007/s00531-016-1390-4

ORIGINAL PAPER

Shallow-generated damage within non-planar strike-slip fault zones: role of sedimentary rocks in slip accommodation, SW Holy Cross Mountains, Poland

Barbara Rybak-Ostrowska[1] · Andrzej Konon[1] · Andrzej Domonik[1] · Anna Poszytek[1] · Joanna Uroda[1]

Received: 15 February 2016 / Accepted: 21 August 2016

Abstract We investigated exhumed damage zones of dextral strike-slip faults dissecting the south-western part of the Mesozoic cover of the Late Palaeozoic Holy Cross Mountains Fold Belt. Structural observations allow to examine the top 1–2 km of the fault zones that deformed asymmetrically with the most intense damage controlled by the non-planar geometry of the faults. The deformational style of fault zones and the roughness of slip surfaces on subsidiary faults within deflections of fault traces in the restraining and releasing bends were facilitated by rock fabric and porosity. High porous sandstones enhanced genesis of cataclastic shear bands within the damage zone and the smooth slip surfaces. Low porous limestones enhanced the formation of dilatant structures infilled with calcite within damage zones and rough slip surfaces. The complex structural pattern of damage zones records multiple episodes of slip and shows evidence of continuous seismic–aseismic modes of fault slip behaviour.

Keywords Fault zone · Shallow generated asymmetric pattern of damage · Rock fabric and porosity · Multiple slip accommodation · Roughness

Introduction

The present study focuses on the influence of rock fabric and porosity on the deformation style of damage zones and the roughness of slip surfaces on subsidiary faults within deflections of fault traces in the restraining and releasing bends of asymmetric strike-slip faults. We propose a methodology of fault zone investigation that allows to interpret the slip accommodation within fault zone and seismic–aseismic behaviour of faults.

The formation of fault zones at shallow depths in crustal conditions is controlled by mechanical properties of rocks and distribution of strain during faulting (Sibson 1977, 1989; Chester and Logan 1986). Lithology and fabric of sedimentary rocks control the internal structure of fault zones (Aydin 1978; Aydin and Johnson 1983; Shipton and Cowie 2003; Micarelli et al. 2006; Bullock et al. 2014; Michie et al. 2014), most often composed of two main units: the fault core consisting of fault rocks such as breccias, gouge, cataclasite or ultracataclasite associated with the slip surface, and the damage zone comprising fractures and subsidiary faults. The two units are separated by a master fault and surrounded by the intact host rock (e.g. Chester and Logan 1986; Caine et al. 1996, 2010; Caine and Forster 1999; Billi et al. 2003; Faulkner et al. 2010). However, the fault zones that lack the cores and damage zones have been recently reported (e.g. Mukherjee 2013a, b, 2015). Natural strike-slip fault zones consist of straight fault segments and deflected parts of fault traces referred to as bends (Harding 1985; Sylvester 1988; Woodcock and Schubert 1994). Numerical simulations incorporating damage rheology governing the seismogenic upper crust display the termination zones of straight fault segments as well as the restraining and releasing bends with significant damage accumulation resulting in a broad damage zone in the top few kilometres of the crust (e.g. Finzi et al. 2009). Intense damage spreads out in the immediate vicinity of the core forming a zone up to a few hundred metres wide. As it moves away from the core, the decreasing strain is accommodated within the several kilometres wide zone (op. cit.).

✉ Barbara Rybak-Ostrowska
barbara.rybak@uw.edu.pl

[1] University of Warsaw, Żwirki i Wigury 93, 02-089 Warsaw, Poland

Published online: 10 September 2016

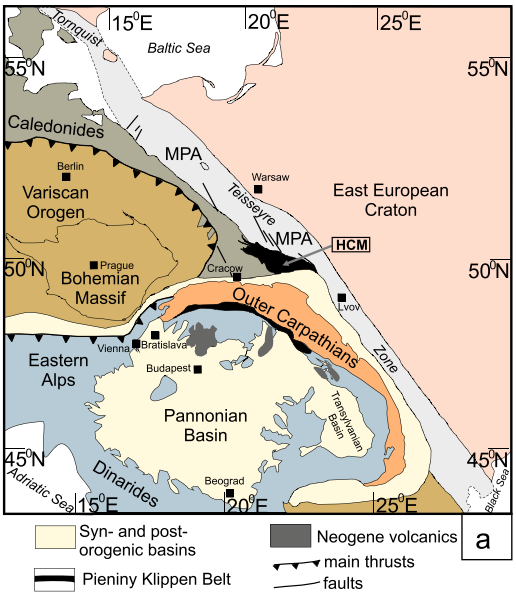
Tornquist
15°E
20°E
25°E
Baltic Sea
55°N
Caledonides
MPA
Berlin
Warsaw
Variscan Orogen
East European Craton
Teisseyre
MPA
HCM
50°N
Prague
Bohemian Massif
Cracow
Lvov
Outer Carpathians
Zone
Vienna
Bratislava
Budapest
Eastern Alps
Pannonian Basin
Transylvanian Basin
45°N
Dinarides
Beograd
Adriatic Sea
Black Sea
Syn- and post-orogenic basins
Neogene volcanics
Pieniny Klippen Belt
main thrusts
faults
a

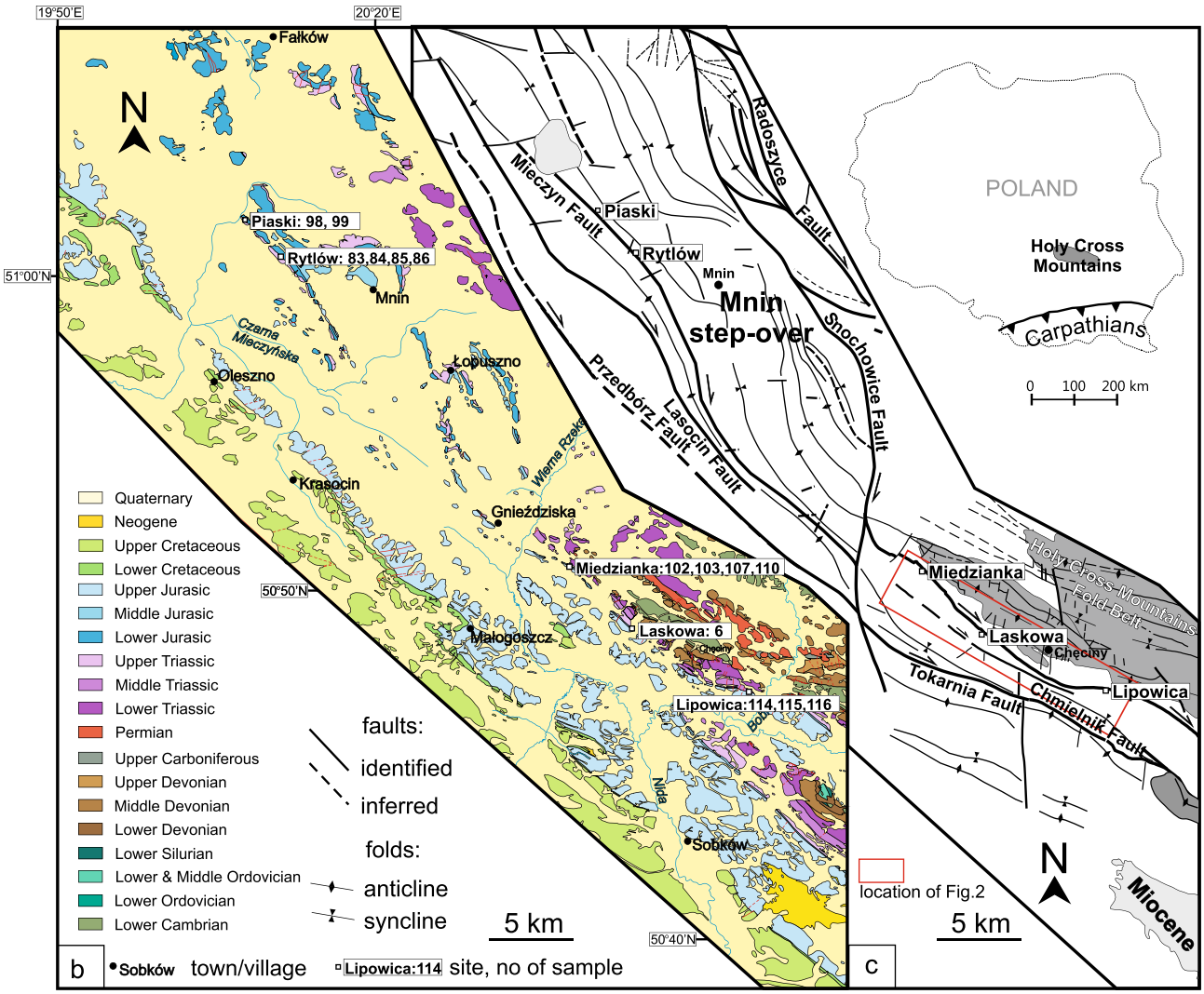
19°50'E
20°20'E
Fałków
N
Piaski: 98, 99
Rytlów: 83,84,85,86
51°00'N
Mnin
Czarna Mieczyńska
Łopuszno
Oleszno
Wierna Rzeka
Krasocin
Gnieździska
Miedzianka:102,103,107,110
50°50'N
Małogoszcz
Laskowa: 6
Chęciny
Lipowica:114,115,116
Bobrza
Nida
Sobków
50°40'N
Quaternary
Neogene
Upper Cretaceous
Lower Cretaceous
Upper Jurassic
Middle Jurassic
Lower Jurassic
Upper Triassic
Middle Triassic
Lower Triassic
Permian
Upper Carboniferous
Upper Devonian
Middle Devonian
Lower Devonian
Lower Silurian
Lower & Middle Ordovician
Lower Ordovician
Lower Cambrian
faults:
identified
inferred
folds:
anticline
syncline
5 km
b
Sobków town/village
Lipowica:114 site, no of sample
Mieczyn Fault
Piaski
Rytlów
Mnin
Mnin step-over
Radoszyce Fault
Snochowice Fault
Przedbórz Fault
Lasocin Fault
POLAND
Holy Cross Mountains
Carpathians
0 100 200 km
Miedzianka
Holy Cross Mountains Fold-Belt
Laskowa
Chęciny
Tokarnia Fault
Chmielnik Fault
Lipowica
location of Fig.2
N
5 km
Miocene
c

◂**Fig. 1** Localization of the study area: **a** tectonic sketch map of Central Europe (simplified after Guterch et al. 2000). *MPA* Mid-Polish Anticlinorium, *HCM* Holy Cross Mountains. **b** Geological map and **c** Fault network of the western and south-western part of the Mesozoic cover of the Holy Cross Mountains (after Czarnocki 1938, 1961; Senkowicz 1958; Jurkiewicz 1961; Krajewski 1961; Różycki 1961; Jurkiewicz 1965, 1967; Filonowicz 1967, 1973; Filonowicz and Lindner 1986; Grzybowski and Kutek 1967; Hakenberg 1973; Szajn 1977, 1980, 1983; Kwapisz 1983; Filonowicz and Lindner 1986; Cieśla and Lindner 1990; Janiec 1991; Mastella and Konon 2002; Konon 2007, 2015)

The rock is strongly fractured within the damage zone that contains subsidiary faults and fractures at different scales, from grain-scale microfractures to macrofractures (e.g. Faulkner et al. 2010). Strains generally concentrate within a narrow segment of the sedimentary cover and form a symmetric damage zone (Finzi et al. 2009). The faults can also separate rocks of differing elastic properties. In this case, shallow-genearated damage may have an asymmetric pattern (Ben-Zion and Shi 2005; Dor et al. 2009).

Although studies addressing the mechanisms of the development of geometrical and structural asymmetries along strike-slip fault zones have often been reported, direct connection with lithological differences remains considerable scientific interest. The subsequent slip along faults tends to produce more planar surfaces and different structural patterns within damage zones. A question arises of the relationship between the structural pattern of damage zones in different lithologies and roughness of fault surfaces at small scale. In addition, the link between the structural pattern of damage zones and the slip mode behaviour of the faults in context of paleoseismicity is still a subject demanding further investigations.

To contribute to a better understanding of the slip accommodation by rocks of different lithologies, we focus on the exhumed damage zones of strike-slip faults dissecting the south-western part of the Mesozoic cover of the Late Palaeozoic Holy Cross Mountains Fold Belt (HCFB) in Poland (Fig. 1a–c) (e.g. Czarnocki 1938; Mastella and Konon 2002). We study the damage zones having an asymmetric pattern along segments of the fault zones where the Gnieździska-Brzeziny and Mieczyn faults juxtapose the strongly differing sedimentary rocks: incompetent Triassic claystones and competent Jurassic siliciclastic and carbonate rocks (Figs. 1b, c, 2). In situ observations in exposures and laboratory studies of subsidiary fault surfaces including microstructural analysis of the damage zones, rock fabric and fault roughness measurements indicate that rock fabric and porosity facilitated the failure patterns of sandstones and limestones and influenced the diverse roughness of the slip surfaces. Moreover, these properties play an important role in slip accommodation and fault development.

Tectonic setting

The study area is located in the transition zone between the Polish and North German basins (e.g. Kutek and Głazek 1972; Ziegler 1982, 1990b; Dadlez et al. 1995, 1997; Krzywiec 2000, 2002; Kutek 2001; Dadlez 2003) and the northern Tethys shelf (Matyja 2009). The Polish and North German basins formed along the Teisseyre-Tornquist Zone (TTZ) and the Elbe Fault System (EFS), respectively (e.g. Dadlez 1997; Scheck et al. 2002; Mazur et al. 2005; Scheck and Lamarche 2005).

The tectonic framework allowed for the formation of a very complex fault pattern within the Permo-Mesozoic rocks unconformably overlying the Palaeozoic basement comprising lower Cambrian to lower Carboniferous rocks of the Holy Cross Mountains Fold Belt (HCFB) (e.g. Czarnocki 1938). The HCFB consists of a series of folds, developed after the Visean, probably during the late Carboniferous and before the late Permian (e.g. Czarnocki 1938, 1950). Map-scale folds, exposed in the fold belt, up to 160 km long and 20 km wide, are cut by map-scale WNW–ESE-striking, longitudinal, and N–S to NNW–SSE-striking, transverse and oblique faults with straight traces (e.g. Czarnocki 1938; Konon 2006, 2007).

In the Permo-Mesozoic strata, west and south of the HCFB (Fig. 1c) dominate NW–SE and NNW–SSE-striking faults, as well as WNW–SSE-striking strike-slip faults forming an anastomosing fault pattern (Czarnocki 1938, 1948; Kutek and Głazek 1972; Konon and Mastella 2001; Mastella and Konon 2002; Konon 2007, 2015).

The strike-slip faulting was related to the inversion of the Polish Basin, as well as the reactivation of the faults belonging to the fault systems of the northern shelf of the Tethys Ocean. The formation of the strike-slip faults resulted from a compressional/transpressional stress regime at the end of the Cretaceous and the beginning of the Cenozoic along the northern Peri-Tethyan Platform (e.g. Ziegler 1987, 1990a, b; Golonka et al. 2000; Dadlez 2003; Mazur et al. 2005). The faults developed when the maximum horizontal compressional stress was ca. 10º (Konon and Mastella 2001; Mastella and Konon 2002).

The fault pattern consists of generally non-planar dextral strike-slip faults (Fig. 1b) (Mastella and Konon 2002; Konon 2015). Similar, not perfectly planar faults are commonly observed along strike-slip fault zones (e.g. Wilcox et al. 1973; Freund 1974; Garfunkel et al. 1981; Heimann and Ron 1987). The strike-slip fault zones with continuously curved traces of faults comprise restraining and releasing bends (e.g. Woodcock and Schubert 1994). Both the restraining and releasing bends were recognized along the Gnieździska-Brzeziny Fault (G-BF) (Konon and Mastella 2001; Mastella and Konon 2002) and Mieczyn Fault (MF) (Konon 2015).

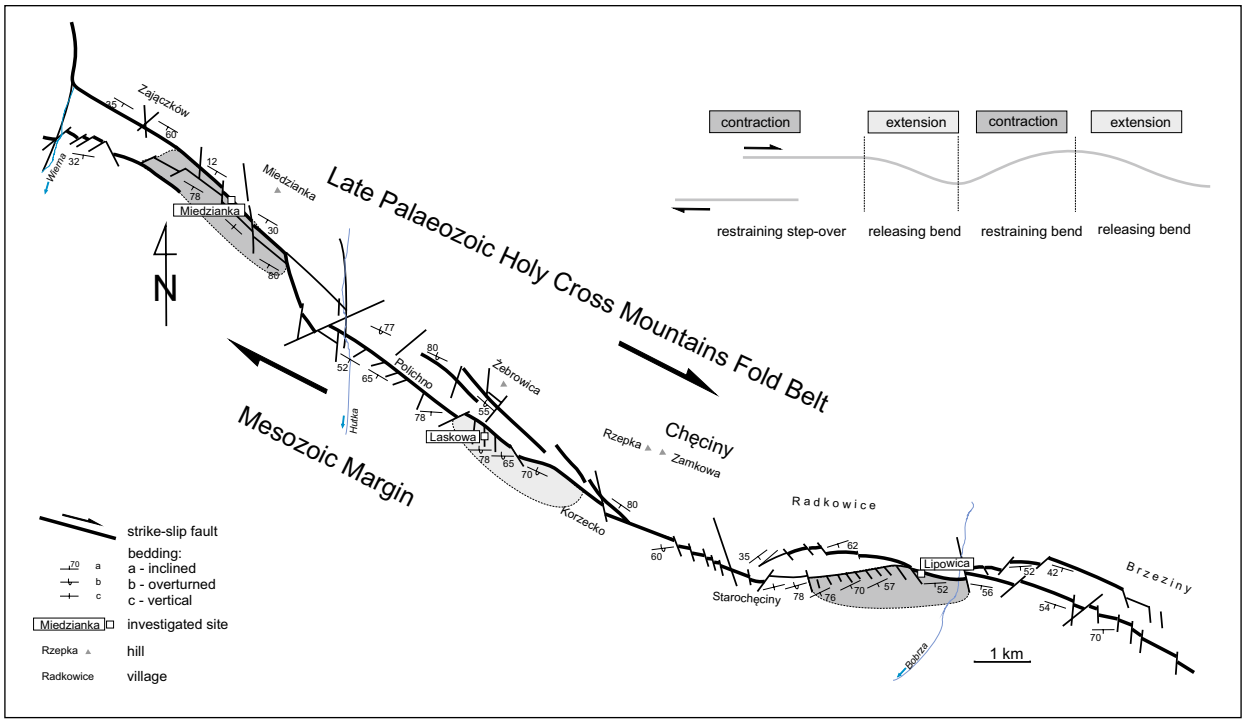

Fig. 2 Non-planar dextral strike-slip Gnieździska-Brzeziny Fault (after Mastella and Konon 2002)

Methods

We have used different methods to obtain detailed characteristics of the fault zones. In situ outcrop observation allowed us to assemble structural data and samples of slickensides and host rocks for further studies. Field studies were coupled with microstructural observations including characteristics of the composition and porosity distribution of the host rocks and structures within damage zones to determine the relationship between the rock fabric and the failure pattern. Additionally, measurements of the slip surface have been used for determining the relationship between the roughness of the slip surfaces and the failure pattern within the sandstones and limestones. The results of these investigations allowed us to complete a conclusion on the role of sedimentary rock fabric on the slip accommodation within fault damage zones.

Fault zone observations and sampling

The structural observations of the Gnieździska-Brzeziny and Mieczyn fault zones have been based on the geological maps at the scales 1:100000 (Czarnocki 1938, 1961) and 1:50000 (Jurkiewicz 1961, 1965, 1967; Filonowicz 1967, 1973; Filonowicz and Lindner 1986; Grzybowski and Kutek 1967; Janiec 1991). Structural observations allowed to examine the top 1–2 km of the fault zones and select representative exposures for the study. The dextral strike-slip fault zones observed in quarries revealed primarily an internal structure of the damage zones of the G-BF and MF. Nevertheless, the exposures lack the main fault planes and the associated cores. As a result, trenches across the fault zones were excavated in two sites: Miedzianka and Lipowica. The trenches revealed the contact between Triassic claystones and Jurassic siliciclastic and limestones (Konon et al. 2016) and exposed the broad damage zones developed in the limestones.

Two different lithologies of sedimentary rocks within damage zones have been selected for sampling (Table 1): medium- and thick-bedded Lower Jurassic sandstones (Piaski and Rytlów), and thin- and medium-bedded Upper Jurassic limestones (Miedzianka, Laskowa and Lipowica). Hand samples of slickensides were collected from subsidiary fault surfaces consistent with Riedel shears (Riedel 1929) along map-scale dextral strike-slip faults from the restraining (Piaski, Rytlów, Miedzianka and Lipowica) and releasing (Laskowa) bends (Figs. 1, 2). The offset of the subsidiary faults varies from few to 10 m.

Samples from Piaski, Rytlów, Laskowa and Lipowica were collected from the first-order R shear with sense of movement consistent with the main dextral strike-slip fault. Samples from Miedzianka were collected from the first-order sinistral R' shear and second-order sinistral R_1' shear (Fig. 3). All samples have been oriented in relation to the subsidiary faults in the field and then to the main MF and GBF (Fig. 3). The samples were analysed to obtain: a

Table 1 Slickenside samples

No.	Localization	Type of exposure	Rocks
6	Laskowa	Abandoned quarry	Limestones
83, 84, 85, 86	Rytlów	Active quarry	Sandstones
98, 99	Piaski	Abandoned quarry	Sandstones
102, 103, 107, 110	Miedzianka	Trench	Limestones, limestones with cherts
114, 115, 116	Lipowica	Trench	Limestones

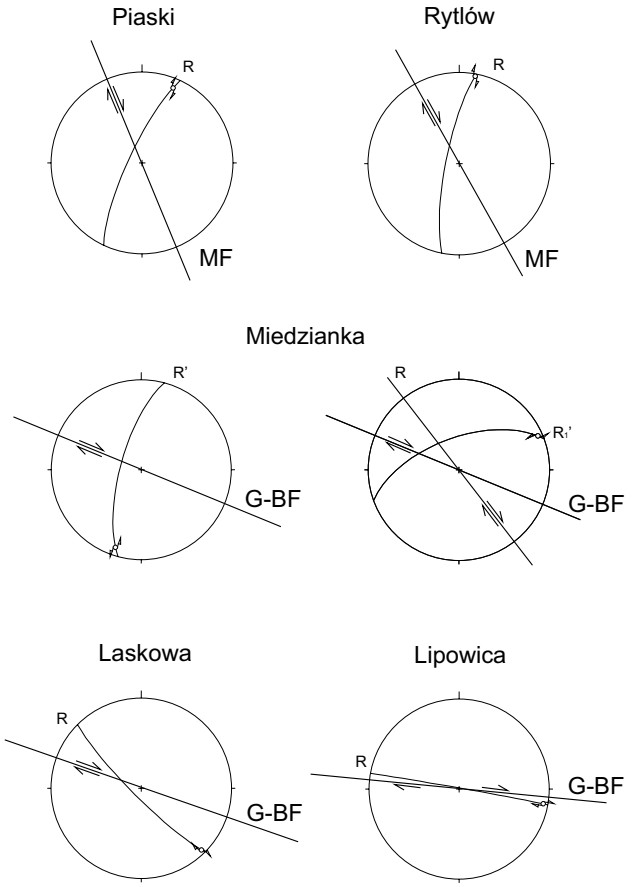

Fig. 3 Diagrams of subsidiary faults related to Mieczyn (MF) and Gnieździska-Brzeziny (G-B) faults

microfracture and microfaults pattern within damage zones associated with the slip surfaces, calcite vein textures, rock porosity distribution within the fault zones and roughness of the slip surfaces.

Microstructural observations

Relationships between the distribution, mineralization of microfracture and microfault patterns, and rock fabric along faults within damage zones have been studied using microstructural observations. They were based on thin sections of representative samples cut along the slickenlines on the fault planes. They were carried out by means of conventional optical microscopy (OM) and scanning electron microscopy (SEM).

Porosity evaluation

Highly porous and cemented low-porosity rocks define various failure patterns. Therefore, the grain size composition, cements and the total porosity of the host rocks have been analysed. Pore distribution data were deduced microstructurally. The samples were impregnated with blue epoxy to show the interconnected pore space in the rock. However, this method was barely useful to analyse limestone porosity due to the microscale of the pores. Therefore, SEM was applied for quantifying microporosity that allowed for the analysis of both interconnected and isolated pores in the rocks. Digital 8-bit image analysis was performed by ImageJ through processing of converted binary images with black pore spaces and the white solid phase of the rocks. Total porosity was defined as the ratio of the sum of the areas from all pores and the entire image area, expressed as the percentage.

Measurements of slip surfaces

The microfracture and microfault pattern within the damage zones, as well as mass transfer within the rocks, may affect the fault surface and produce different roughness. Results of field measurements of fault surfaces from other areas indicate distinct roughness recognizable at various scales (e.g. Power et al. 1988; Renard et al. 2006; Candela et al. 2009). For this study, we have used laboratory measurements of roughness in small segments of rock samples obtained from the fault surfaces. A contact profilometer was used to obtain images and quantitative parameters of the investigated segments of the fault surfaces. The Hommel Tester T800 profilometer is a measuring instrument used to analyse a surface profile to quantify its roughness. A rigid steel stylus equipped with a sapphire blade is moved vertically in contact with a sample and then moved laterally across the sample for a specified distance and specified contact force. A profilometer measures small surface variations in a vertical stylus displacement as a function of position. The device was set to measure vertical features ranging from 10 to 10 mm in height. The height position of the

stylus generates an analogue signal (magnetic induction), which is converted into a digital signal that is stored, analysed and displayed by additional software (HommelMap and Turbo Roughness). The radius of the applied sapphire blade is 20 nm, and the horizontal discretization (spacing between the profiles) is 10 μm. The stylus tracking force was in the range of 0.6–2.5 mN. To measure surface roughness, experiments were conducted on 14 small segments (30 × 30 mm) of rock samples under identical conditions. Each investigated surface consisted of 300 single profiles.

Measurement of the roughness parameters was carried out in accordance with DIN EN ISO 4287 specification (2010) and EUR 15178 EN report (1993). Total roughness statistical parameters (S_a, S_q, S_{sk}, S_{ku}) and additional amplitude parameters (S_t, S_p, S_v) are described and presented below.

S_a—the arithmetic mean of the sum of the values of roughness profiles:

$$S_a = \frac{1}{NM}\sum_{x=0}^{N-1}\sum_{y=0}^{M-1}\left|z_{x,y}\right|$$

Statistically, S_a is the arithmetic mean of the deviations of the roughness profiles about the centre line. S_a provides limited information because of its sensitivity to extreme peaks and valleys in the profiles.

S_q—the root-mean-square roughness is defined as the value obtained from the deviations of the roughness profiles over the surface (square values of the peaks):

$$S_q = \frac{1}{NM}\sum_{x=0}^{N-1}\sum_{y=0}^{M-1}z_{x,y}^2$$

In practice, S_q is the measure of the standard deviation of the profile angle and is more sensitive to extreme peaks and valleys than S_a.

S_{sk}—the measure of the shape or symmetry or symmetry of the amplitude density curve of the roughness profiles:

$$S_{sk} = \frac{1}{NMS_q^3}\sum_{x=0}^{N-1}\sum_{y=0}^{M-1}z_{x,y}^3$$

A plateau-like profile is indicated by negative skewness values. A normal distribution of the profile values results in zero skewness. Skewness values are greatly influenced by individual extreme profile peaks and valleys.

S_t is the total height of the surface. It is the height between the highest peak and the deepest valley. S_p is the highest peak of the surface. It is the height between the highest peak and the mean plane. S_v is the deepest valley of the surface. It is the depth between the mean plane and the deepest valley.

Characteristics of the damage zones

Exposures of the Mieczyn fault zone show well-preserved damage zones covering the sandstones. Small quarries along the Gnieździska-Brzeziny Fault zone reveal damage zones covering the limestones. The width of the damage zones is limited by the size of the exposure and attains up to several metres for the sandstones and up to 20 m for the limestones. Trenches excavated at the Miedzianka and Lipowica sites have revealed that the fault zones are composed of three lithological complexes: (1) incompetent claystones exceeding several metres, (2) a mixed zone of claystones and elongated or lens-shaped fragments of competent gaizes arranged parallel to bedding that ranges in width from a few to several metres; and (3) a damage zone covering the limestones that exceeds 25 m in width (cf. Krauze 2015). In the study, we focus on the shallow generated brittle failure of the rocks that concentrated within the damage zones developed in sandstones and limestones (Figs. 4, 5, 6, 7, 8).

Structural features

The strong failure of rocks within damage zones exposed in the Piaski, Rytlów, Miedzianka and Lipowica sites denote restraining bends (Figs. 1b, 2, 4a, 5a, 6a, 8a). A weaker damage of the overturned beds in the Laskowa site denotes a releasing bend (Figs. 2, 7a), where macroscopically the rocks seem to be almost intact. Intense damage of rocks at this site is recognizable exclusively in microscale. Cross sections of rocks cut parallel to the striation show details of slip surfaces and associated damage zones with shear fractures and their infillings. They contain minor structures that correspond to the sense of movement of the sampled faults recognized during field work. Hence, characteristics of the internal structure of damage zones within sandstones and limestones require detailed mezo- and microstructural observations discussed in the following sections.

Sandstones

The sandstones are strongly affected by subsidiary faults and shears development resulted in complex structural pattern of damage zones recognizable macroscopically at both Piaski and Rytlów sites. Slickensides developed within the sandstones are highly polished, grooved and corrugated along the slip direction (e.g. Means 1987). The slickensides are intersected with synthetic Riedel shears (Petit 1987; Doblas 1998) that resulted in incongruous steps (Figs. 4, 5). Cross sections parallel to the grooves on the slickensides within sandstones show thin, up to 4-mm-thick zones

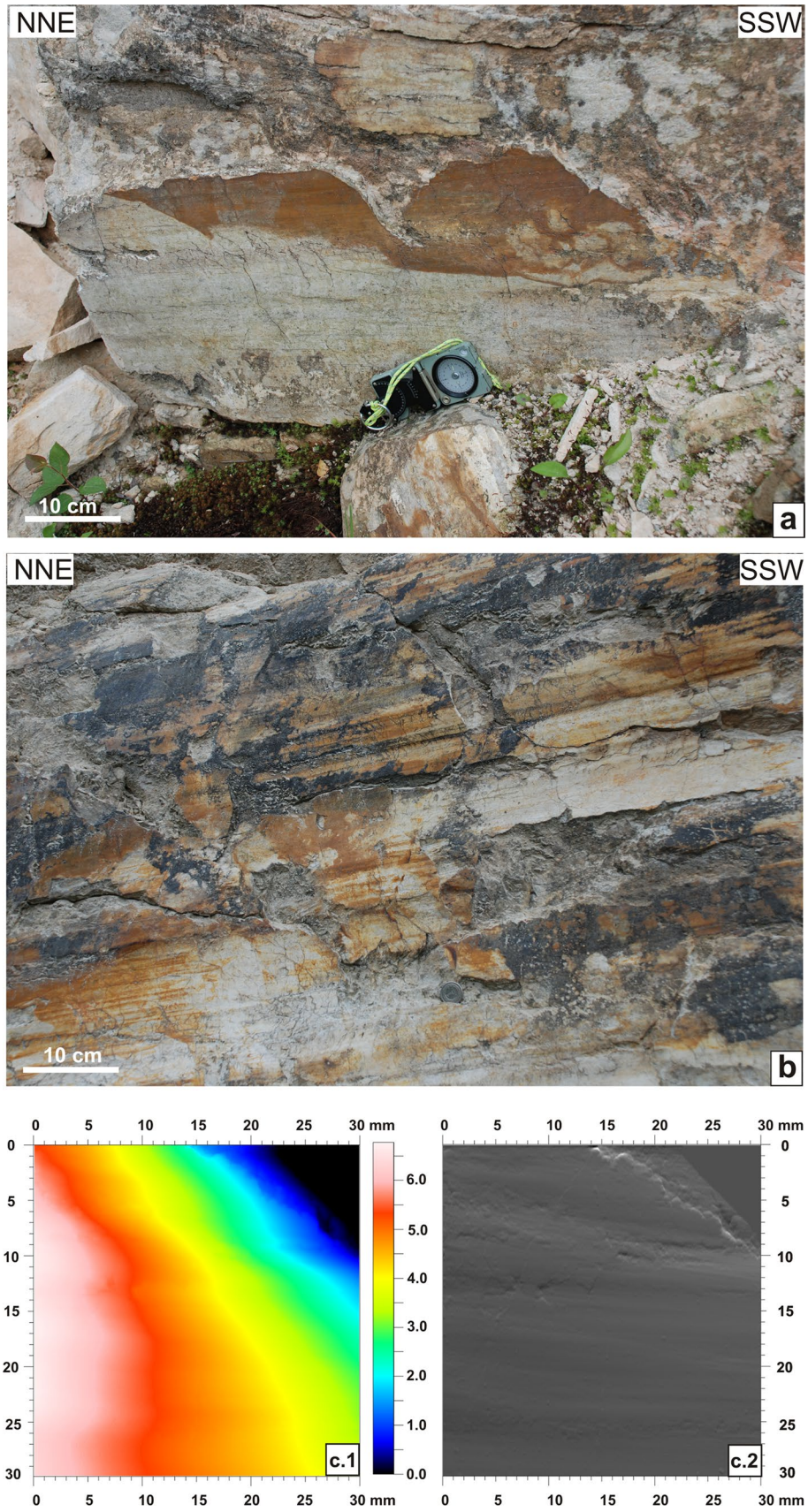

Fig. 4 **a**, **b** Slickensides from dextral R subsidiary faults of Mieczyn Fault zone cutting lower Jurassic sandstones at Piaski. **c** Visualization of roughness of slip surface: *1* topography map, *2* 2D diagram (pseudo-image)

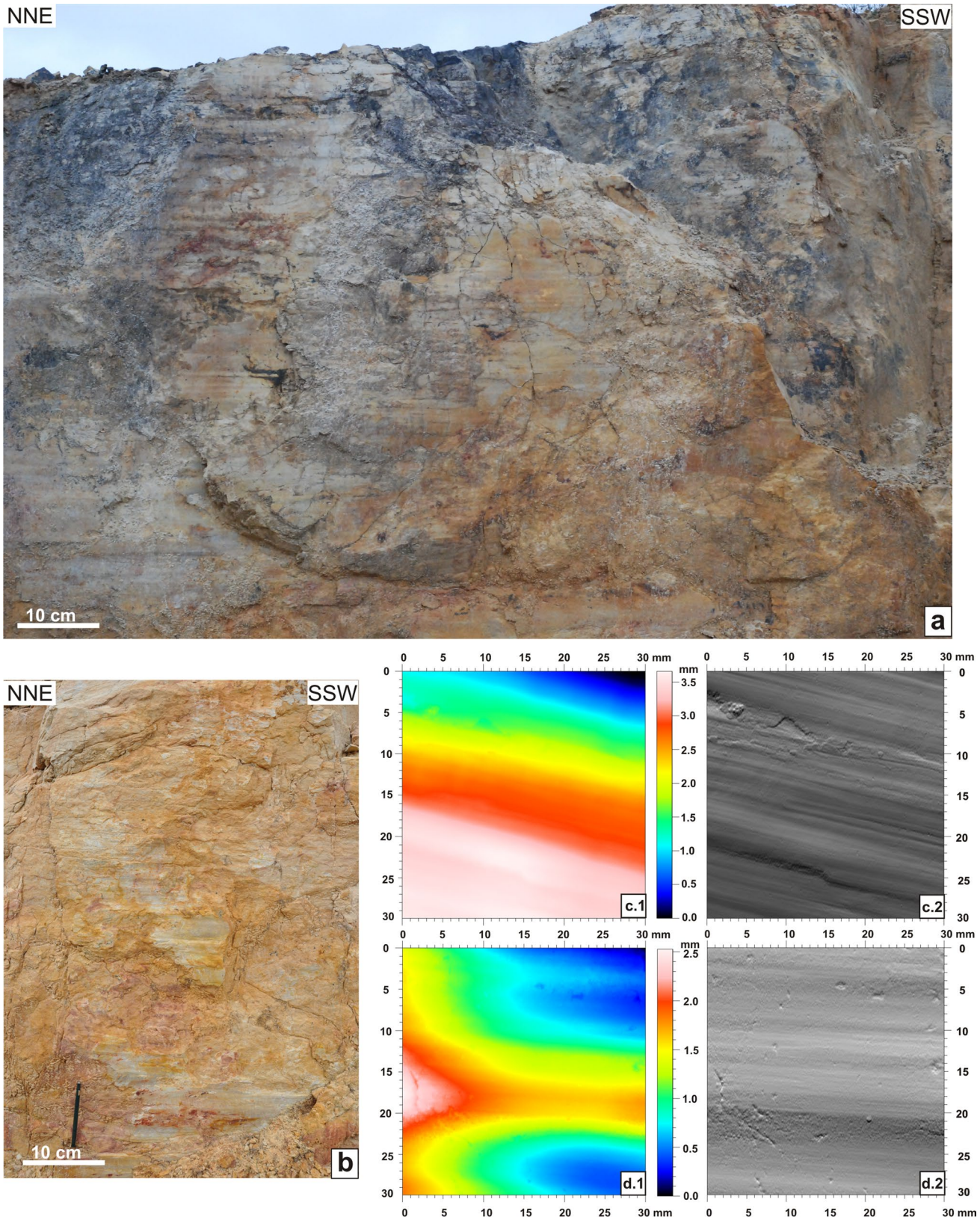

Fig. 5 **a**, **b** Slickensides from dextral R subsidiary fault of Mieczyn Fault zone cutting lower Jurassic sandstones at Rytlów. **c**, **d** Visualization of roughness of selected slip surfaces: *1* topography maps, *2* 2D diagrams (pseudo-images)

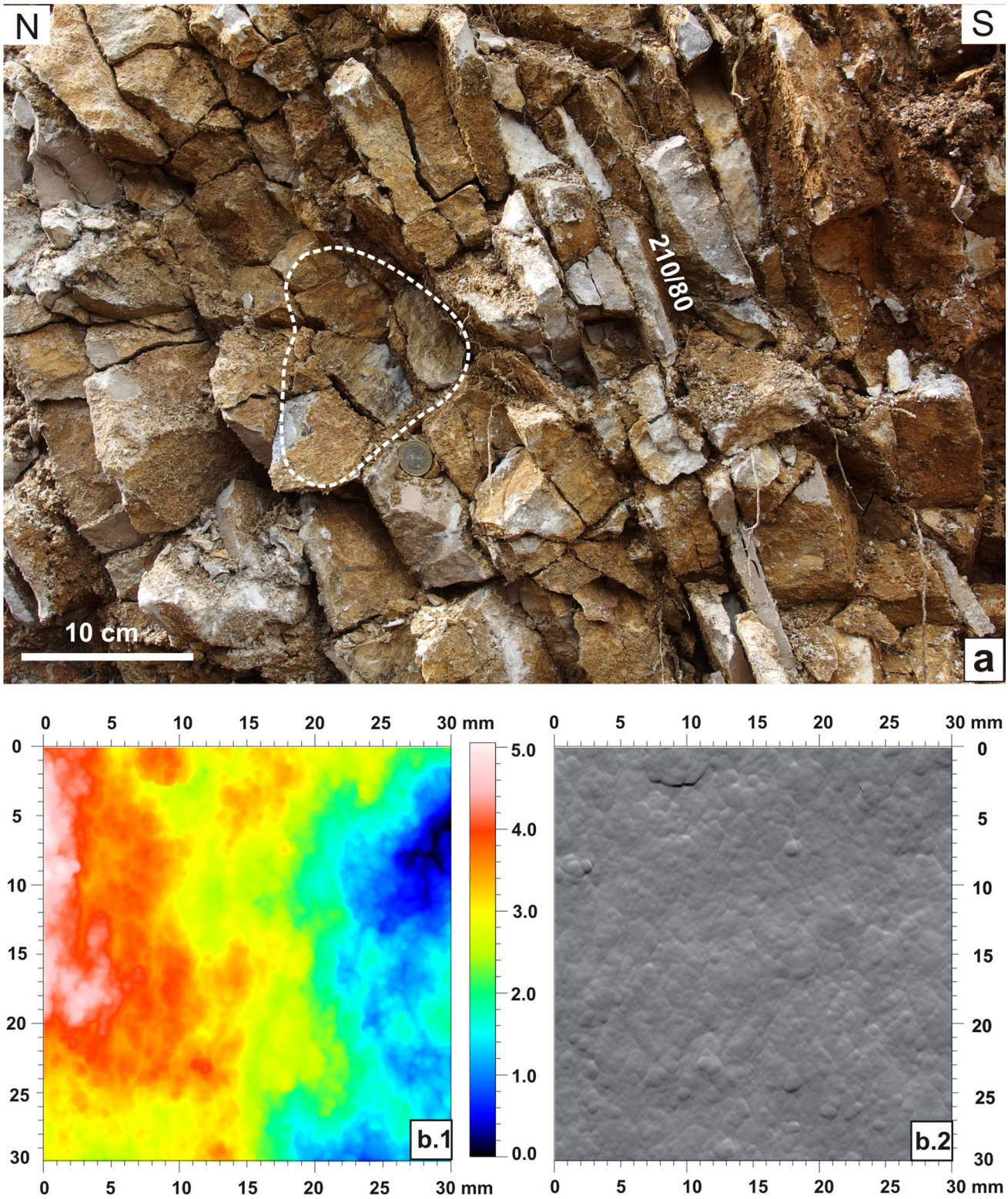

Fig. 6 **a** Slickenside from sinistral R′ subsidiary fault from intensively damaged upper Jurassic limestones within Gnieździska-Brzeziny Fault zone at Miedzianka. **b** Visualization of roughness of slip surface: *1* topography map, *2* 2D diagram (pseudo-image)

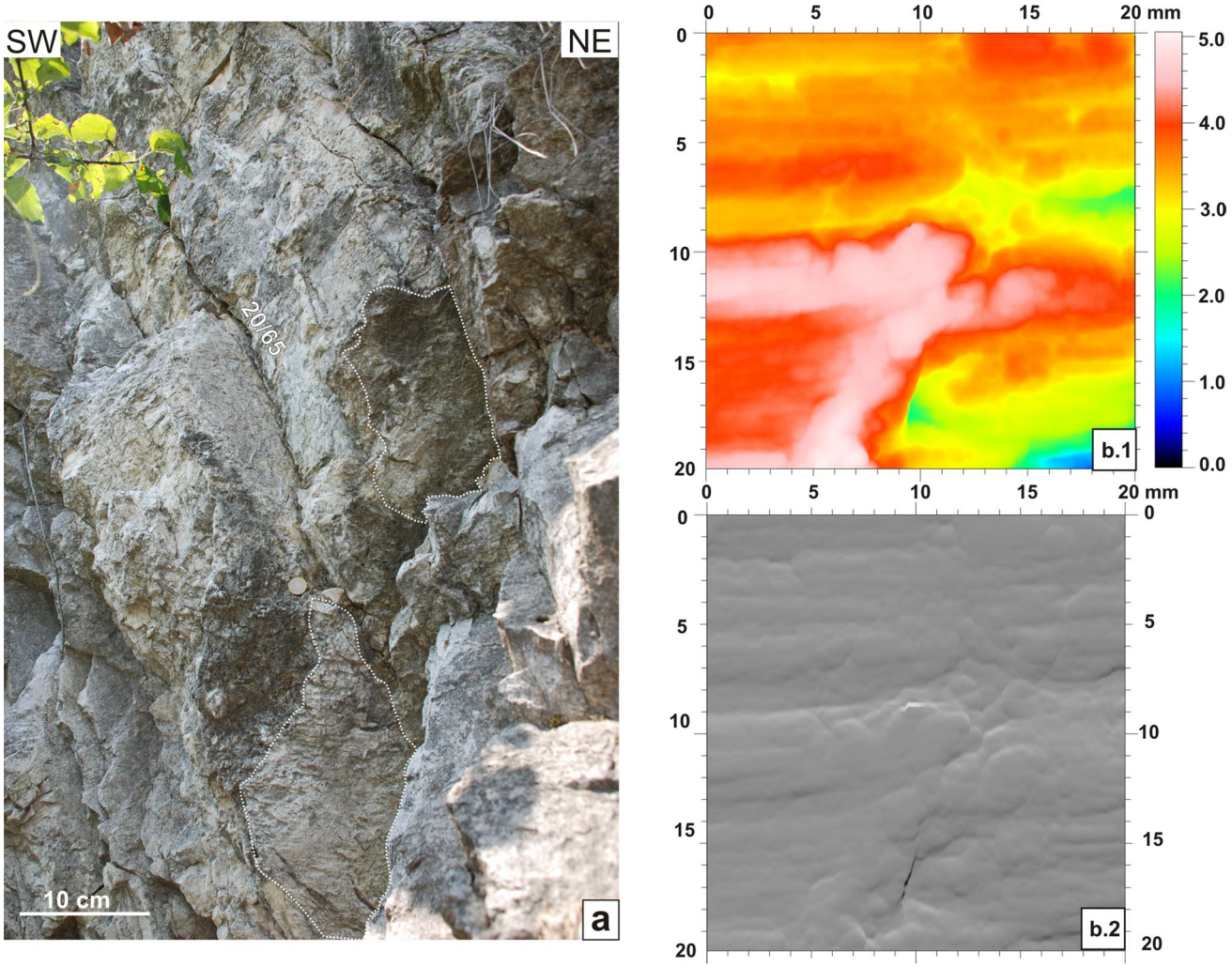

Fig. 7 **a** Slickensides from dextral R subsidiary fault from Gnieździska-Brzeziny Fault zone at Laskowa. **b** Visualization of roughness of slip surface: *1* topography map, **2** 2D diagram (pseudo-image)

of fault rocks that can be traced continuously along the exposed fault plane.

Cross sections of damage zones, limited to tens of centimetres in width, show very thin, up to 2-mm-thick deformation bands or clusters of bands that are arranged parallel or oblique to the main slip surface in wall damage zones (Fig. 9). They also occur in the continuation of the main slip surface within the host sandstones in the tip damage zone. The deformation bands result in low and high angle patterns of the Riedel shears. The deformation bands are brighter in colour, more cohesive and more rigid in comparison with the intact host rock.

Deformation bands observed within sandstones sites occur in three sets (Fig. 9): (1) parallel to the main slip surface and synthetic to the sense of movement of the sampled fault that corresponds to the Y shears, (2) inclined at 50°–80° to the slip surface with the sense of movement hardly recognizable macroscopically that geometrically corresponds to the *R′* shears, and (3) two opposed sets with an inclination 15°–25° to the slip surface and synthetic to the sense of movement of the sampled fault that correspond to R and P shears, respectively. The shears developed within individual sets or more often coexist within complex networks that show geometrical and kinematical relationships with the fault damage zone. Spacing between the individual shear fractures in the sets ranges from few millimetres to centimetres (Fig. 9a–d) and depends on the density of slip surfaces within a multilayered fault zone. Macroscopically, the R bands tend to show a slightly variable (15°–25°) angular position with respect to the fault plane and a distinct linear or segmented geometry within the damage zone. Such angular relation conforms with the field observations from other areas (e.g. Mukherjee and Koyi 2010; Mukherjee 2010, 2013a, b). It is significant that this type of Riedel shears may be linked to the P or Y deformation bands within a very narrow, up to few centimetre

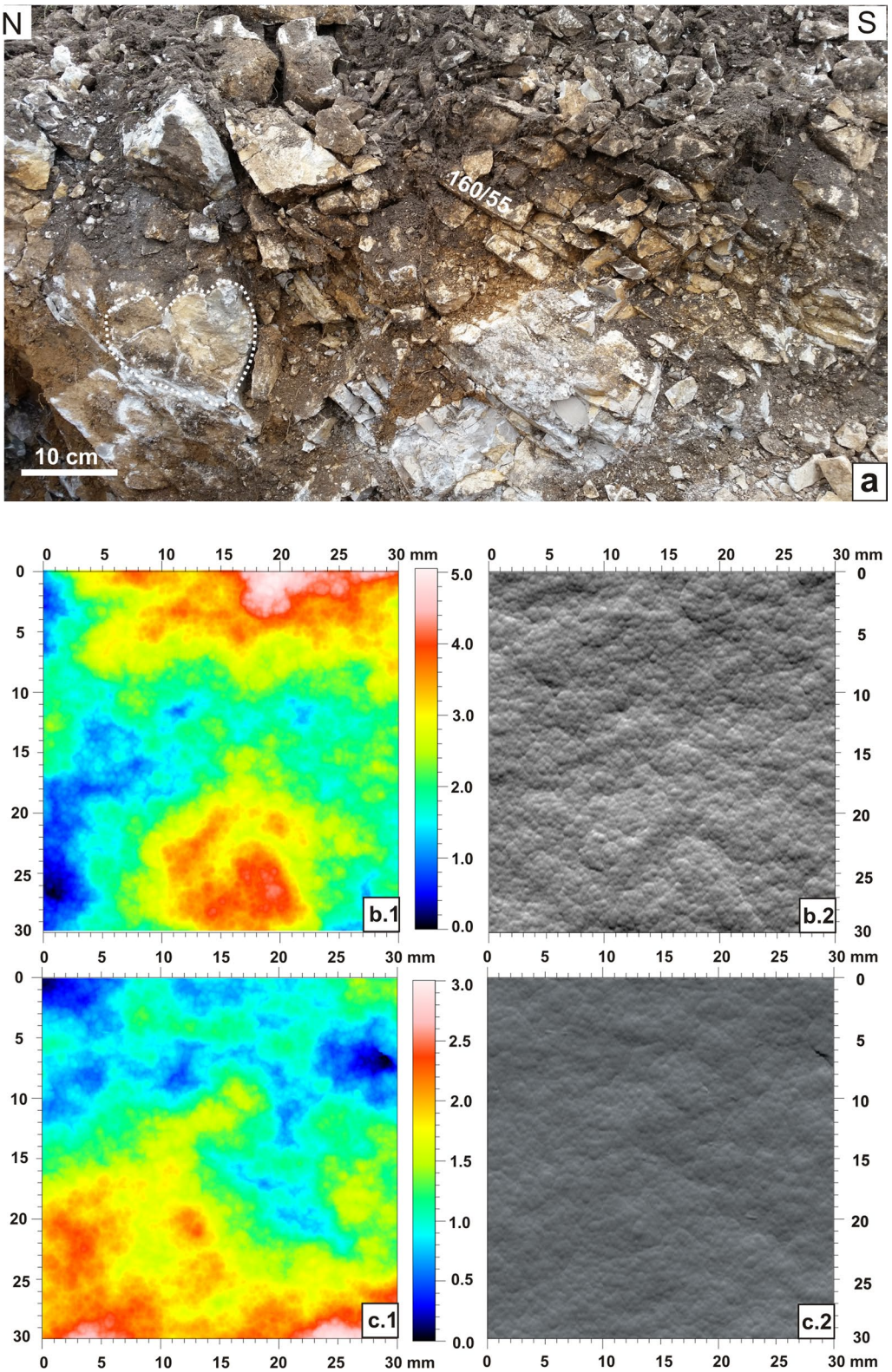

Fig. 8 **a** Slickenside from dextral R subsidiary fault within Gnieździska-Brzeziny Fault zone cutting upper Jurassic limestones at Lipowica. **b**, **c** Visualization of roughness of slip surfaces: *1* topography map, *2* 2D diagram (pseudo-image)

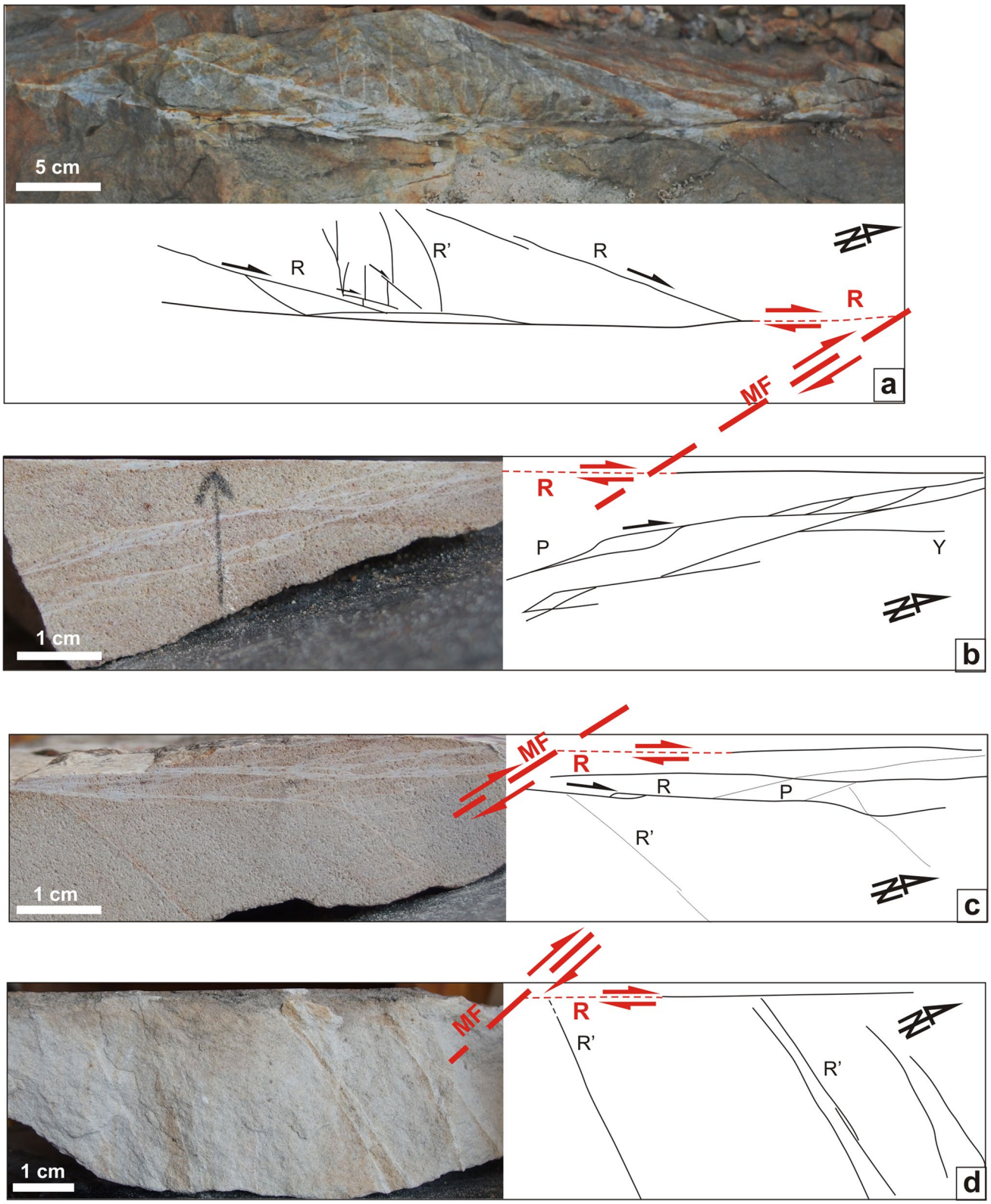

Fig. 9 Structural pattern of deformation bands associated with subsidiary fault zones: **a**, **b**, **c** Rytlów, **d** Piaski. *MF* Mieczyn Fault

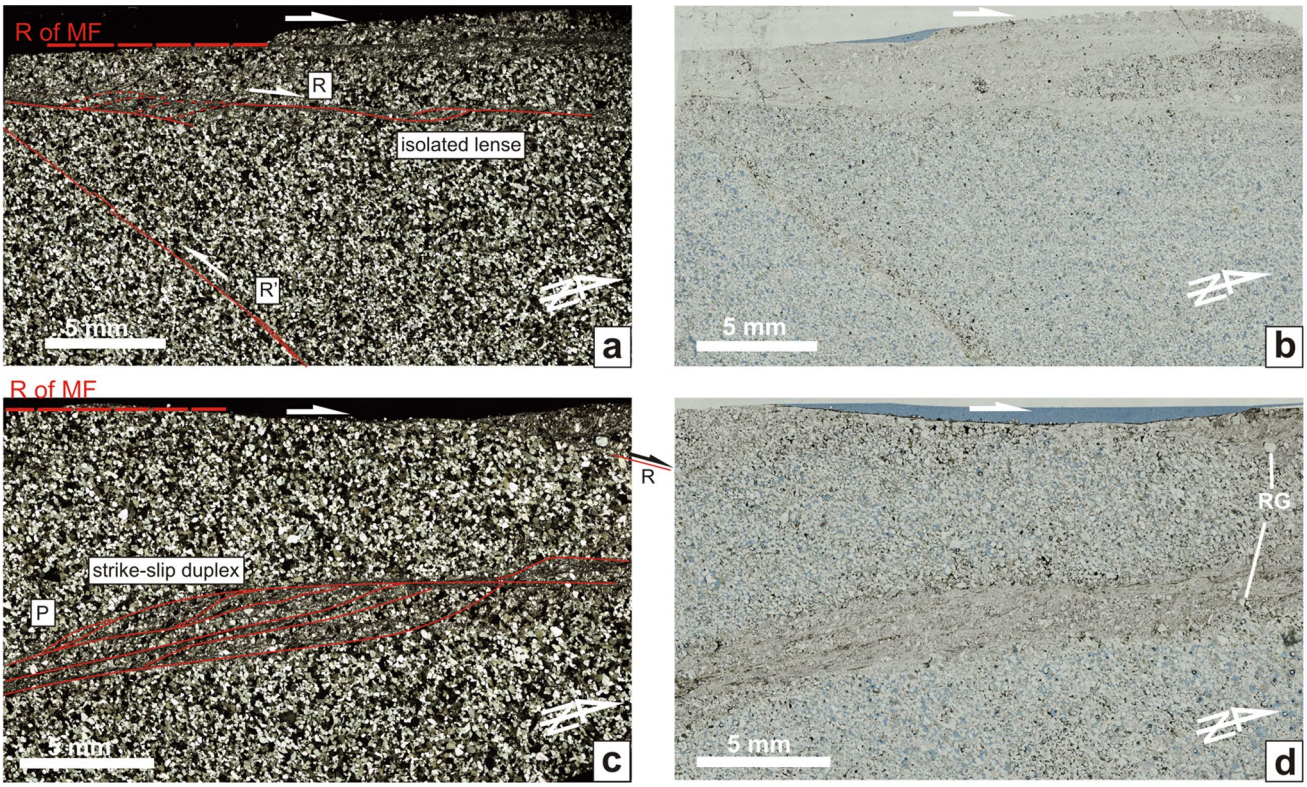

Fig. 10 Internal structure of cataclastic shear bands within sandstones at Rytlów based on OM images. **a**, **c** Details of geometry and kinematics of shear bands. **b**, **d** Grain size and porosity reduction within shear bands in relation to host sandstone. Relicts of intact grains (RG) within shear bands can be seen. Sense of movement based on field observation. *Light* **a**, **c** cross-polarized; **b**, **d** plane polarized

wide zones that covers the area in the close vicinity of the fault surface. R' deformation bands show a slightly curved or rarely sigmoid geometry and a quite narrow lateral distribution. It is significant that the R' deformation bands tend to change the angle of inclination to the fault plane from 45° to 85° with an increasing complexity of the structural network within the damage zones. Low-angle R' sets commonly occur individually and terminate on the fault surface or on the R, P deformation bands (Fig. 9a, c). The high-angle R' sets occur individually or more often develop between R shears (Fig. 9a, c). Some cross sections of the damage zones show that the R shears cut and offset the *R′* shears (Fig. 9a).

Thin sections of sandstones within the fault zones show that the fault rocks and thin bright deformation bands consist of cataclasites (Figs. 10a–d, 11a, b). Based on the deformation mechanism depending on the composition, grain size, porosity and cementation of the deformed rocks, the deformation bands have been defined as cataclastic bands (Aydin 1978; Aydin and Johnson 1983). The presence of small-scale kinematic indicators, described further in the text below, allows us to classify them as compactional shear bands (after Aydin et al. 2006).

Shear bands occur individually, coalesce within the anastomosing pattern or are arranged in discrete arrays (Figs. 9, 10). Additionally, they form clusters within the array oversteps. Shear bands have a limited length and tend to bifurcate at their ends. Their thickness ranges from 0.05 to 1 mm. Shear bands form zones that can be up to 15 mm in width. Spacing between shear bands within the zones varies from tenths of a millimetre up to a few centimetre. They commonly display a small-scale fault stepping geometry that allows to establish kinematic indicators (Fig. 10a, c) in form of isolated lenses (e.g. Fossen and Hesthammer 1997) and strike-slip duplexes within clusters (e.g. Woodcock and Fischer 1986; Cruikshank et al. 1991). Both structures occur within contractional oversteps of bands that form linking damage zones. The individual parallel bands within the structures delimit isolated fragments of the host sandstones that bear a primary texture or are partly deformed. This resulted in a small-scale shear band-bounded sandstone compartments texture. The structure contains lenses of preserved or slightly deformed host rocks.

The contact between the cataclasites and the host rock is distinct (Fig. 10a–d, 11a). The mineral composition of the cataclasites along the slip surface and shear bands is the

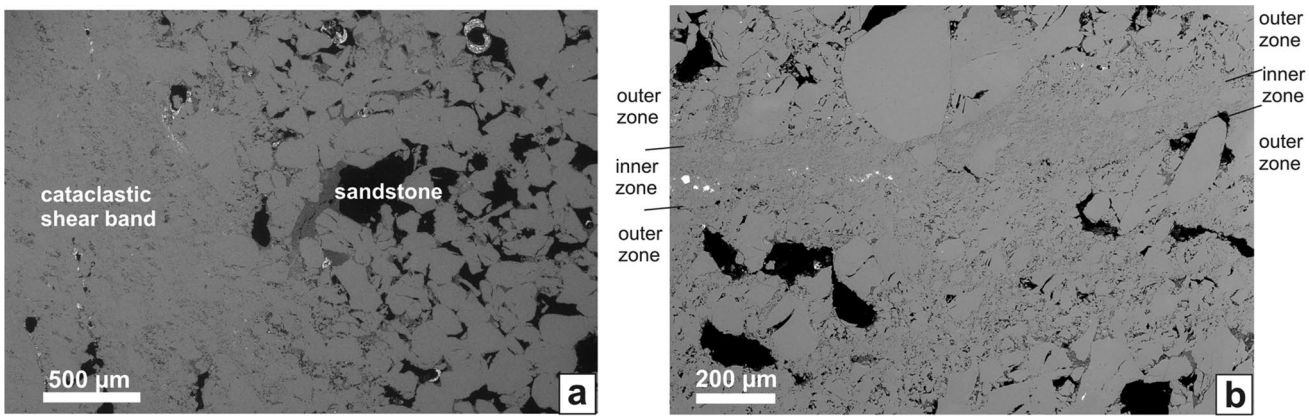

Fig. 11 Examples of grain and porosity distribution within shear bands from Rytlów based on SEM images: **a** contact between shear band and host sandstone; **b** bisected structure of shear band with significant fragmentation of grains resulted in fine-grained cataclasite within inner zone and coarse-grained cataclasite within outer zone

same as the host sandstones. Cataclasites consist of grains of finer fractions (0.01–0.1 mm), and the intergranular space contains very fine and predominantly angular or slightly rounded, elongated, crushed fragments of larger grains, loosely distributed in the clay-siliceous matrix (Fig. 11a, b). The crushed grains show a various level of damage across the bands with fracture propagation limited to individual grains. The orientation of grain fracturing is predominantly subparallel to oblique with an inclination of 10°–40° with regard to the shear bands extent (Fig. 11b). Fractures are intragranular of mode I—wedge-shaped, often limited to a part of the grain, and mode II—cross-cutting the grains (Fig. 11b). Fracture propagation and distribution resulted in grain size reduction. The fragmented grains within the shear bands are arranged subparallel (smaller fragments) or slightly oblique (larger fragments) to the shear band extent. Residual grains of the host rock have been noted within the shear bands. Some of the shear bands display a bisected structure with a distinct inner and outer zone (Fig. 11b), respectively, of stronger and weaker comminution of grains (cf. Aydin and Johnson 1983; Underhill and Woodcock 1987). Processes of fragmentation and comminution of grains provided matrix formation that caused porosity reduction within the deformation bands to 0.5–4 %, in relation to the host sandstone (Figs. 10a–d, 11a, b) with the highest reduction within the inner zone of the structures. The porosity is very fine intergranular with no visible evidence of dissolution.

Limestones

The limestones are strongly fractured and fragmented within the fault zones exposed at Miedzianka and Lipowica that resulted in tens of metres broad damage zone. Fragmentation of beds within some parts of damage zones is so strong that bedding can be barely seen (Fig. 6). The fractured rocks commonly occur as lens- or sigmoid-shaped fragments. Conversely, the limestones exposed at Laskowa show overturned beds with weak macroscopic damage in relation to the Miedzianka and Lipowica (Figs. 6, 7, 8). The beds can be traced continuously across the site and are slightly fractured. Slickensides developed within limestones at all sites show a mineral lineation, striation and/or different types of steps, both congruous and incongruous, resulting most often from the development of Riedel-type shears and calcite-infilled extensional fractures (Figs. 6, 7, 8). The slip surfaces and the shear fractures within damage zones are usually associated with calcite mineralization with bulk within the main fault. Host limestones with cherts bear structures less mineralized by calcite in comparison with those within pure limestones. The mineralized fractures and shears intersected with slickensides form a visible network of asperities.

Cross sections of slickensides from subsidiary faults within limestones show fault rocks that represent microbreccias (Fig. 12a, c). The rocks display an abundance of the calcite assemblage within veins of fragmented host rocks and a network of thin, up to 0.5-mm-thick fractures and shears that divide the host rocks into smaller fragments. Slip surfaces within limestones are underlined by calcite veins with fibrous crystals that extend predominantly parallel to the slip surface (Fig. 12b) or with blocky or elongated crystals also arranged subparallel or slightly oblique to the slip surface (Fig. 13a, b). Additionally, limestones with cherts can form clear-cutting slip surfaces without a mineral infilling or with a small assemblage of calcite along some parts of the fault plane (Fig. 14a, b).

Thin sections of damage zones within limestones display a complex structural pattern dominated by extensional and shear structures accompanied by calcite growth (Figs. 13, 14, 15).

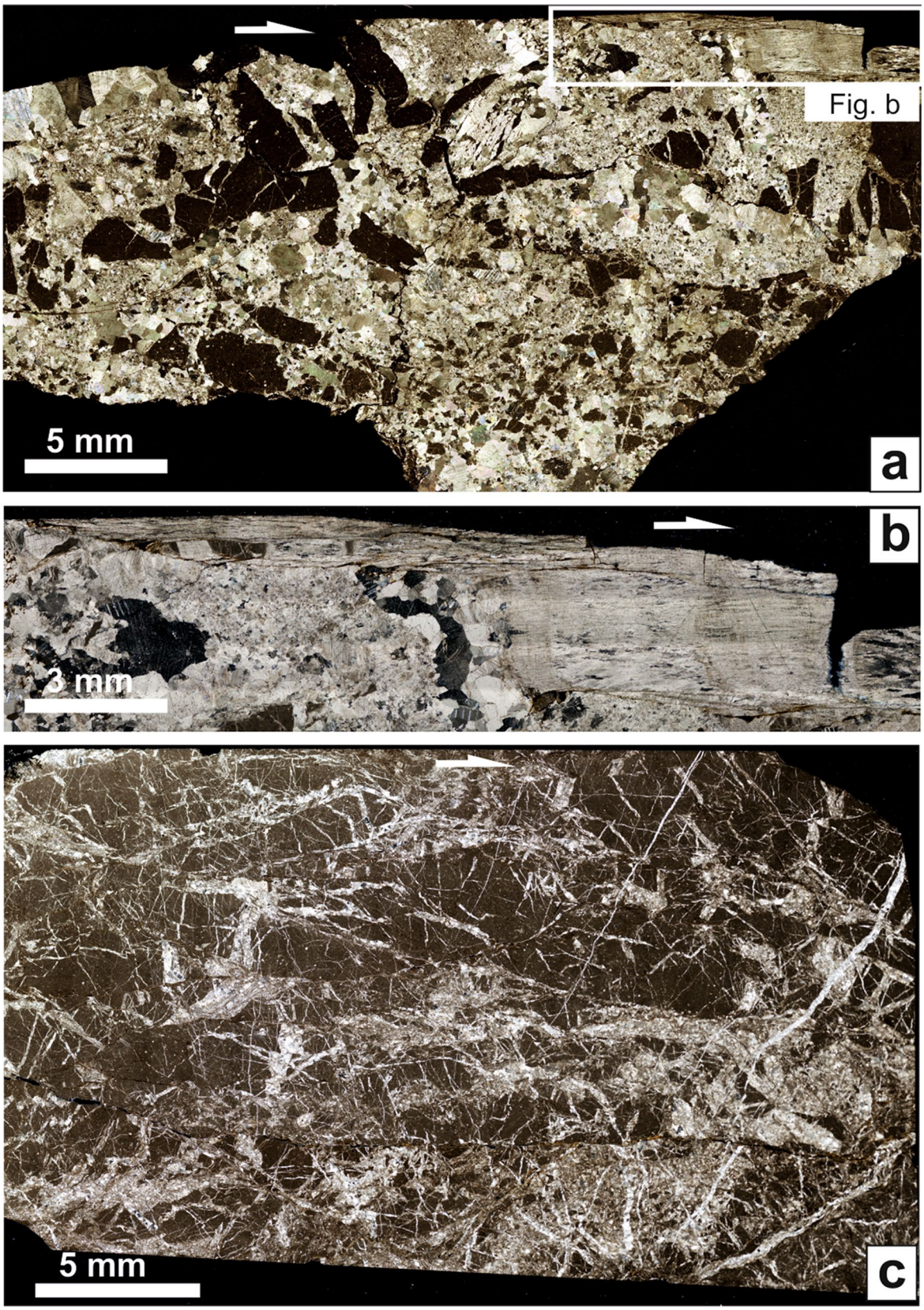

Fig. 12 Fault rocks within fault zones cutting limestones: microbreccias from **a** Laskowa and **c** Lipowica, with abundant assemblage of calcite. **b** Fragment of fibrous calcite vein parallel to fault plane. Sense of movement based on field observation. Cross-polarized light

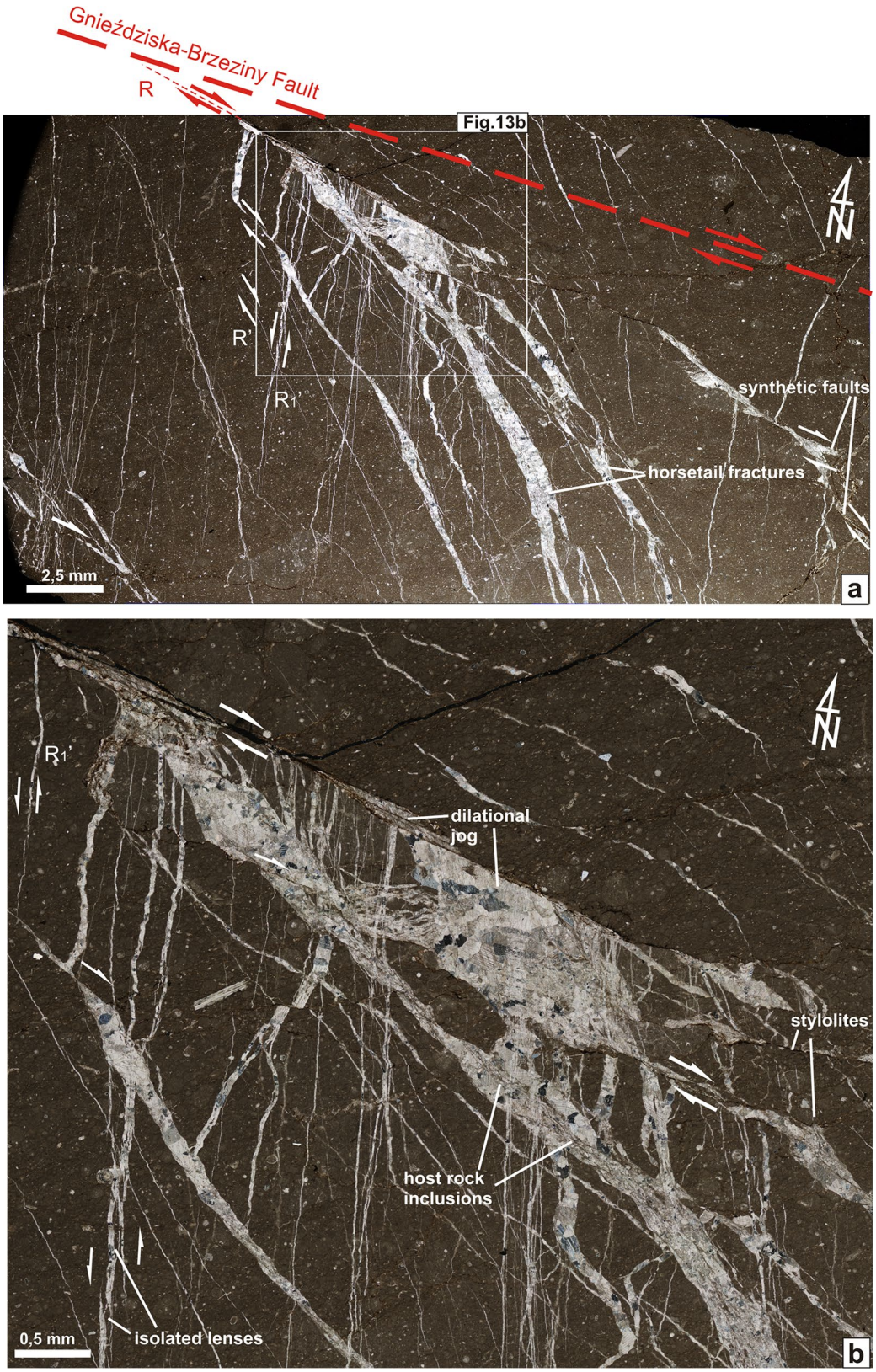

Fig. 13 Complex structural pattern of damage zone of dextral strike-slip fault cutting limestones at Lipowica. Sense of movement of the main fault based on field observation. Cross-polarized light

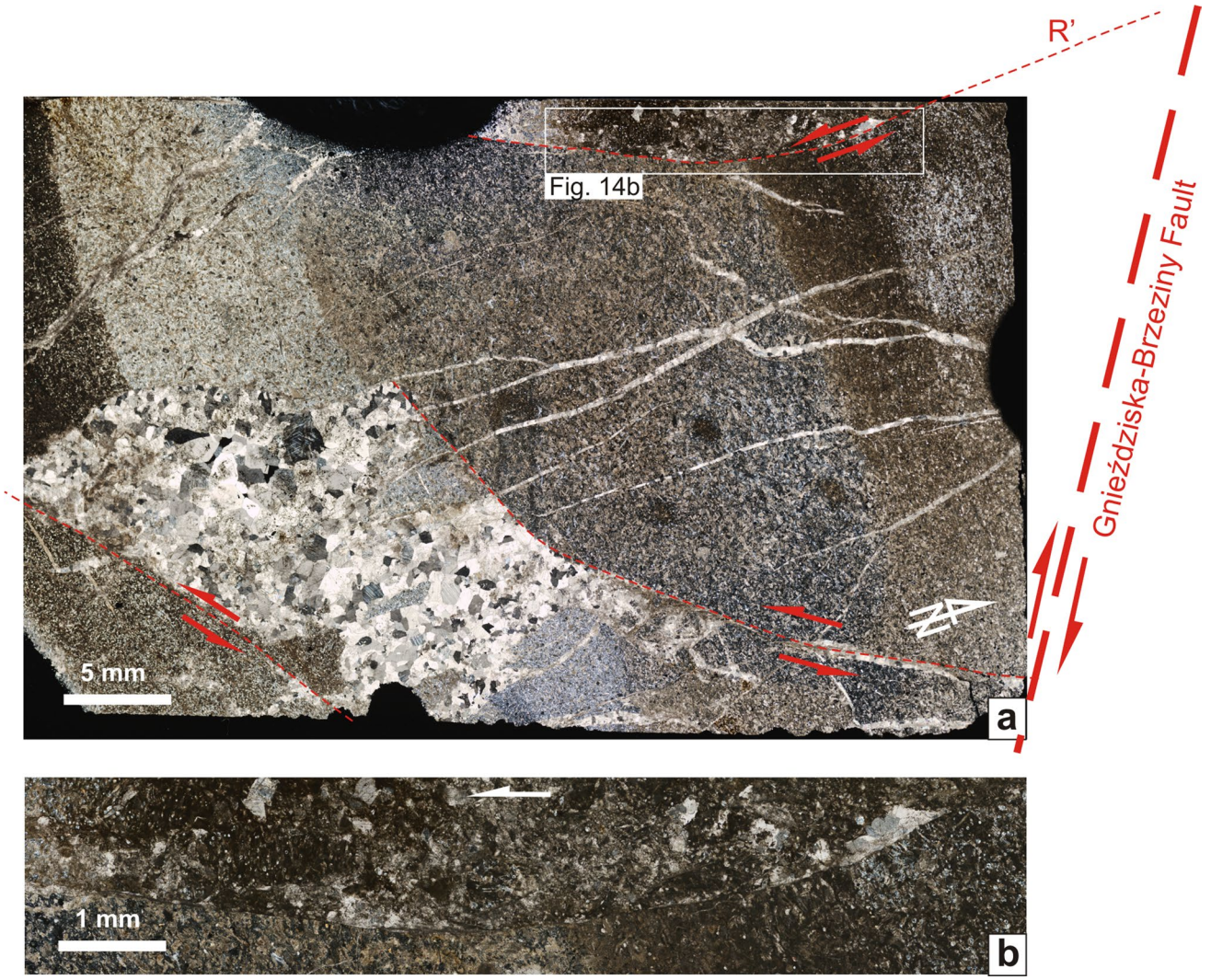

Fig. 14 Calcite veins within limestones with cherts from Miedzianka: **a** Network of syntectonic veins within damage zone. The *grey–blue* automorphic silica occupies parts of the sample. **b** Details of clear-cutting fault plane. Sense of movement based on field observation. Cross-polarized light

Segmentation of microfaults resulting in extensional overstepping geometry is common (Fig. 13). The steps between individual segments show dilational jogs of various width and length that exceeds up to few millimetres. The steps with densely arranged segments produce very thin and relatively long dilational jogs predominantly infilled with fibrous calcite arranged parallel to the segments (Fig. 13a, b). In turn, greater spacing between the segments facilitates the formation of relatively larger dilational jogs with blocky and elongated calcite arranged slightly oblique to the jog walls and subparallel to the segments. The geometry of these structures depends on the wall morphology of the extension fracture that preceded jog development. It is often reflected by narrow inclusions of the host rock that are up to a tenth of millimetre wide, arranged parallel to the wall rock (Fig. 13b).

The tip damage zones are dominated by horsetail fractures inclined at 50°–60° to the slip surface and wing cracks inclined at 40°–45° to the slip surface (Fig. 13a). Those are 0.2–1.0 mm thick. The horsetail fractures tend to have a wavy, occasionally curved wedge-like shape and are subdivided by synthetic microfaults arranged subparallel or slightly oblique, up to 5°, to the main slip surface. The microfaults form a dense pattern in the close vicinity of the main slip surface that dies out towards the intact host rock (Fig. 13b). The displacement along the faults resulted in the dilational pattern of the calcite veins with blocky and elongated crystals arranged subperpendicular to the

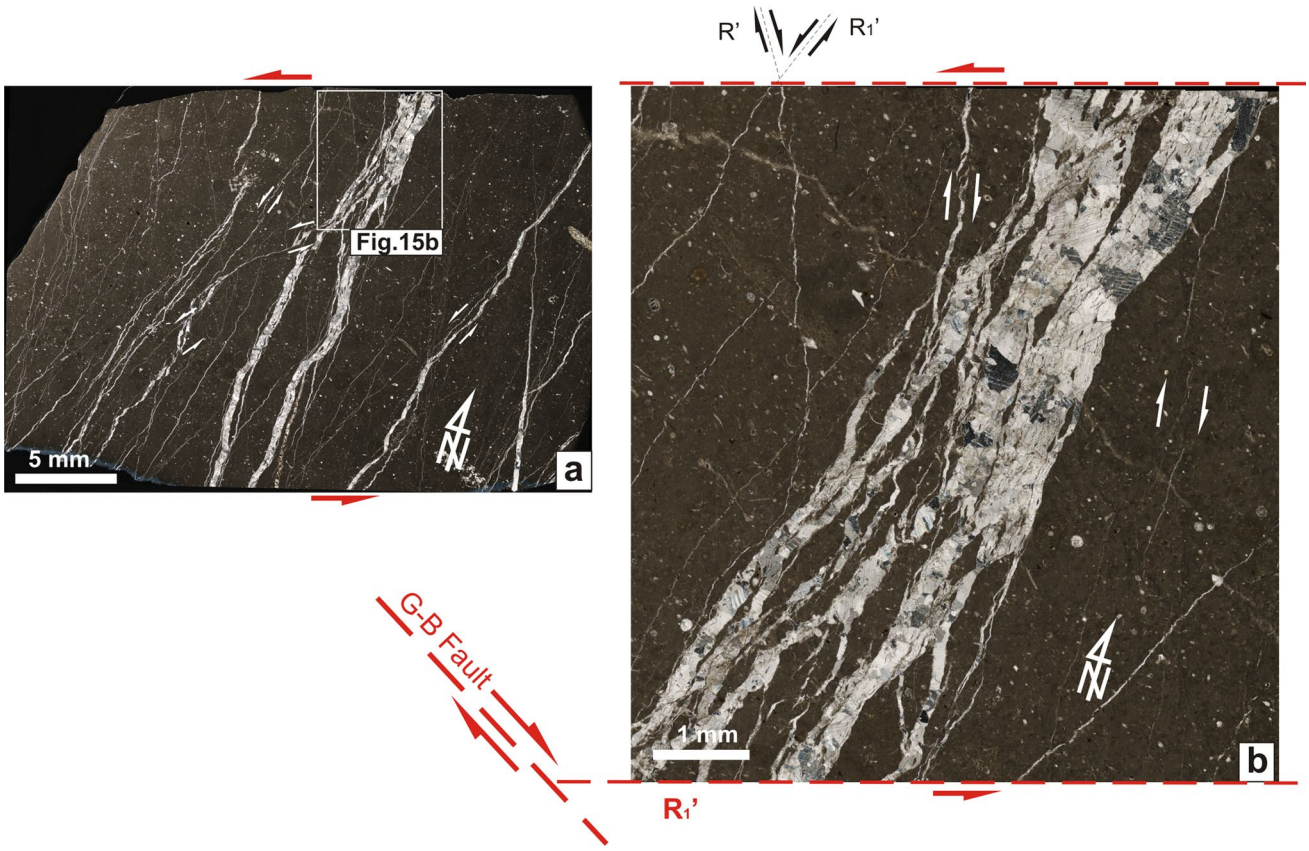

Fig. 15 Shear fracture network infilled with calcite developed within limestones at Miedzianka. Sense of movement based on field observation. Cross-polarized light

fracture wall. Similarly to the previously described veins within the oversteps, the veins contain host rock inclusions that extend along the veins between synthetic faults and reflect the fracture wall geometry. Such a pattern resulted in a complex vein texture that changes across the damage zone (Fig. 13b).

Wall damage zones display shear fractures that tend to occur in one or two sets (Figs. 13, 14a, 15). Individual shear fractures within the sets are inclined at different angles: 15°–20°, (Fig. 15a), 60°–80° (Fig. 15a) and 80°–85° (Fig. 13a), to the slip surfaces. The sense of movement is synthetic in the first set and antithetic in the two other sets, corresponding to R, R' and R_1' shears. The shears begin from the slip surfaces and continue into the host rock for a limited length of up to tens of centimetres. Their thickness ranges from a few millimetres near the slip surface to zero at the end. Some of the steep shear fractures occur in an echelon pattern with closely spaced, calcite-infilled arrays that are lozenge or sigmoidal in shape (Figs. 13a, b; 15a, b). They crosscut larger dilational jogs, horsetail fractures and other shear fractures within the complex damage zones (Fig. 13). The arrays show extensional oversteps. Occasionally, neighbouring arrays are connected and form isolated lenses (Figs. 13, 15). The thickness of an individual array exceeds 0.2 mm, whereas its length varies from tenths of a millimetre to tenths of a centimetre. Other shear fractures extend continuously across the damage zone and show a complex multilayered structure built by minor calcite veins divided by host rock particles incorporated into the structure (Fig. 15). The veins show a wavy, band-like geometry. An individual vein can bifurcate into a cluster of thinner veins and coalesce again into one or two veins. Some of the veins occur along minor segmented faults and thus form a step-like morphology (Fig. 15b). The thickness of the veins reaches up to 1.0 mm.

The development of calcite crystals within shear fractures resulted in the same pattern as within the horsetail fractures or dilational jogs. They are blocky or slightly elongated and do not exceed 1.0 mm in size. They are arranged subperpendicular or slightly oblique to the vein walls. Commonly, individual crystals continue across the veins and cover several host rock inclusions (Fig. 15b). The

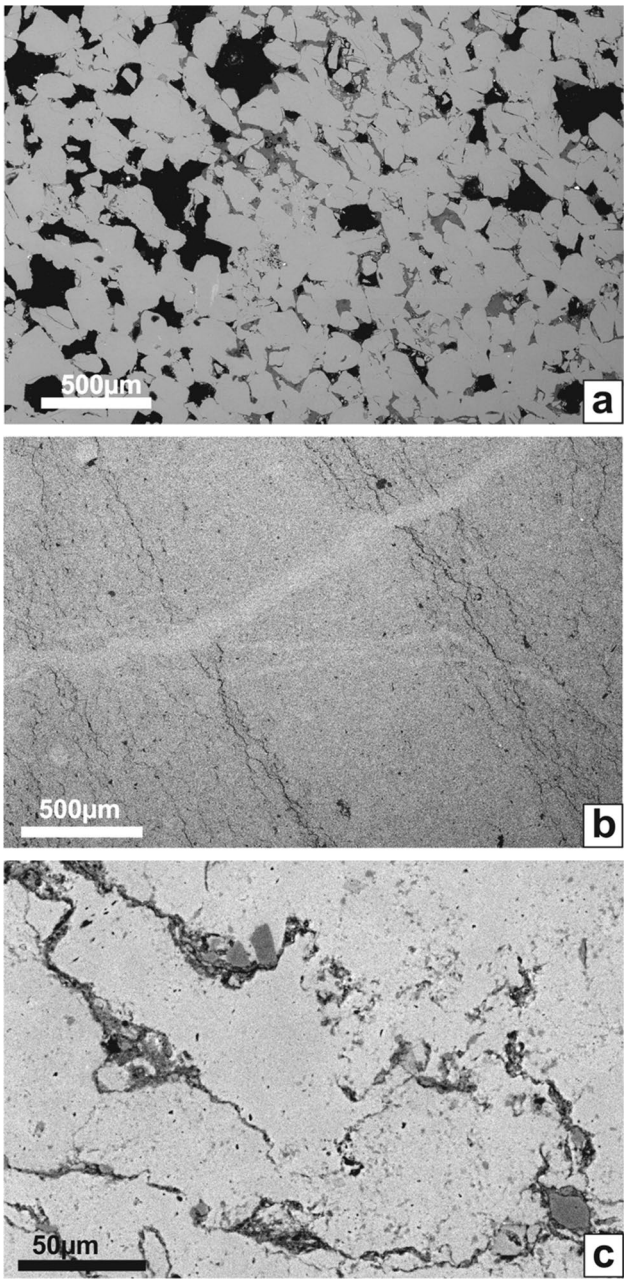

Fig. 16 Examples of rock fabric and porosity distribution based on SEM images: **a** sandstones at Rytlów; **b**, **c** limestones at Lipowica

shape of the inclusions is lozenge-like and wavy, sometimes sigmoid, with the longer boundary reflecting the geometry of the vein wall.

Most of the veins within damage zones display secondary deformation textures. Deformation lamellas within primary calcite crystals are common (Figs. 13, 14, 15). Pressure solution seams occur at the boundaries of rock fragments within the breccias, extend along and parallel to the slip surfaces and across the damage zones (Figs. 12, 13, 16).

Rock fabric characteristics

Rock fabric analysis has been performed for a better understanding of the failure mechanism within the sandstones and limestones.

Sandstones

The sandstones represent fine-grained quartz arenites (after Pettijohn et al. 1972) with grain-supported texture. The rock fabric is characterized by well-preserved primary structural features with partly fractured grains and high porosity (Fig. 16a). Grains are rounded, but the bigger grains are much more angular than the smaller grains. Grains are medium sorted with a size variation between 0.1 and 0.3168 mm. The predominant grain size is 0.20–0.25 mm. The bigger and smaller grains contribute to ca. 30 % grains in the samples. The rock fabric contains only a small contribution of the quartz cement that resulted in significant porosity. The sandstones show two types of porosity: primary porosity restricted by mechanical compaction and cementation, and secondary porosity related to grain dissolution. The primary porosity is partly cemented by early quartz, up to a few per cent. Early cementation is evidenced by the dominance of point and straight grain contacts resulted from low mechanical compaction. The total porosity of the rock fabric is 15–22 %.

The fabric and high porosity of the sandstones facilitated cataclastic flow during faulting: frictional sliding and grain crushing within thin localized zones of slip resulted in shear bands formation. Quartz grain fracturing resulted in grain comminution and matrix formation within the shear band network. Quartz cementation completed the previous mechanical porosity reduction.

Limestones

The limestones are developed as mudstones and grainstones (after Dunham 1962) with massive texture (Fig. 16b) and irregular silica concentrations interpreted as cherts. The silica occurs also as the partial infilling of stylolites (Fig. 16c). Image analysis indicates that the rock fabric is characterized by very low porosity, not exceeding 0.1 %. This is intercrystalline porosity chaotically distributed in the rock as fine, isolated pores that are better developed in grainstones than in mudstones. Most probably, the development of this porosity is related to the early phases of diagenesis. Much higher values of porosity were observed in the case of fissure porosity accompanying stylolites, developed independently from the rock fabric porosity. It reaches 3 % and is composed of a network of interconnected fine fissures. Stylolites contain also pores formed due to dissolution of the stylolite mineral infilling.

Table 2 Results of the measurement of the roughness parameters

Parameters	No. of sample									
	Sandstones					Limestones				
	83	85	86	98	99	102	110	114	115	116
S_a (mm)	0.832	0.431	0.426	1.443	0.369	0.754	0.672	0.442	0.854	0.715
S_q (mm)	0.964	0.527	0.5	1.614	0.452	0.902	0.854	0.523	0.985	0.916
S_{sk}	−0.587	−0.024	0.206	−0.744	−0.248	0.323	0.239	0.364	0.267	0.233
S_p (mm)	1.19	1.43	1.38	2.69	1.04	2.29	2.40	1.67	2.83	2.37
S_v (mm)	2.47	1.34	1.15	4.09	1.21	2.22	2.24	1.33	1.96	2.61
S_t (mm)	3.66	2.77	2.53	6.78	2.25	4.51	4.64	3.00	4.79	4.98

The low porosity of the cemented limestones and their massive texture facilitated brittle failure and formation of extensional structures during faulting. The presence of tectonic stylolitic seams associated with small-scale structures within damage zones suggests syntectonic pressure solution mass transfer from the host rocks towards the extensional structures resulting in syntectonic calcite growth.

Roughness of slip surfaces

Quality assessment of the roughness of the sampled fault surfaces confirms that the surfaces are less rough within sandstones than those within limestones (Figs. 4, 5, 6, 7, 8). The visible nivelation of the asperities on the slickensides within sandstones resulted in their lower roughness. Nevertheless, the grooves and ridges produced a strongly determined lineation that allowed to establish the direction of movement.

The quantity assessment of the roughness (Table 2) reveals that S_a and S_q—the arithmetic mean and the quadratic mean—indicate that in both cases, the peaks on the analysed fault planes have an even statistical distribution. Based on their values, it is not possible to conclude on the differences in roughness between limestones and sandstones, but they indicate that the peaks and valleys have a normal (Gaussian) distribution on the measurement plane.

In turn, distinct differences in S_{sk} values allow to determine the symmetry of the profile ordinate distribution. Negative S_{sk} values reflect the prevalence of valleys over peaks and indicate the concentration of material in the vicinity of small peaks, which points to a 'plateau-like' surface. Such case is observed clearly in sandstones. In four out of five samples, the S_{sk} values are negative (Table 2) and the plateau-like surface incised by narrow valleys is visible also on maps and pseudo-images (Figs. 4, 5). In the case of limestones, the S_{sk} values are positive, indicating the predominance of peaks over valleys (Figs. 6, 7, 8).

Additional parameters confirm this observation. S_p, ordinates of the highest peaks, does not exceed 1.5 mm in sandstones and is much larger in limestones (Table 2). Valley depths (S_v) are similar in both cases, whereas a similar relationship as for S_p was observed for S_t, because this is the sum of the height of the highest peak and the depth of the lowest valley on the surface ($S_p + S_v$).

The analysis of roughness indicates that the slip surfaces within the sandstones are smooth with well-developed grooves and ridges along the slip direction. The slip surfaces within the limestones are relatively more rough with high widespread peaks.

Discussion

The investigation of non-planar dextral strike-slip fault zones shows an asymmetric pattern of failure within both restraining and releasing bends resulting from different properties of rocks within the fault walls. Shallow generated brittle failure of rocks was concentrated within the southern walls built of competent sandstones and limestones exposed, respectively, along the Mieczyn and Gnieździska-Brzeziny faults. The relatively uniform trend of the deformational pattern of sandstones within all localities is correlated with the location within the restraining bend of the studied section of the fault. The more diversified trend of the deformational pattern in limestones is associated with the non-planar geometry of the studied sections of the fault. The intensity of damage is related to the geometry of the fault and depends on the position within the contractional and extensional sectors of the fault. Contractional sectors of faults show intense macro- and microscopically recognizable damage zones with intense crushed rocks cut by numerous subsidiary faults (Figs. 6a, 8a, 12c), whereas extensional sectors show the formation of subsidiary faults with microscopic-scale rock crushing resulting in the formation of microbreccias. This regularity can be interpreted as perturbations of fault geometry and partial accommodation of fault slip by intense damage of rocks within contractional sectors of the fault.

Multiple episodes of fault slip have facilitated a distinct, complex structural pattern within the damage zones

developed in sandstones and limestones exposed along a fault zone that is recognizable in macro- and microscale. Results of the detailed analysis of the studied fault zones are consistent with the previous worldwide studies in fault zones (e.g. Johansen et al. 2005; Fossen et al. 2007; Blenkinsop 2008; Faulkner et al. 2010) and provide evidence for two distinct deformation styles of fault development with regard to rock fabric and porosity.

Deformation of highly porous sandstones (Figs. 9, 10, 11) is primarily dominated by a micromechanism of grain crushing and shearing that resulted in the formation of shear bands and intense pressure dissolution of grains within the host rock without mass transfer into the shear bands. Cataclastic shear bands (Figs. 10a, c; 11a, b) exhibit grain fracturing, comminution, matrix development and cementation that reduce porosity in relation to the intact host rock (Fig. 11a–d). The presence of cataclasis, strong cementation and cluster patterns probably facilitated slip that developed along the shear bands, often at their boundaries, and continued as segments within the shear band or propagated across the clusters of shear bands within oversteps of segments (cf. Knipe et al. 1997; Hesthammer and Fossen 2001; Nicol et al. 2013). The complex structural pattern of the damage zones within sandstones comprising Riedel shears indicate a successive, multistage evolution of the fault zones from low-angle R' through R associated with high-angle R' or P shear bands (Fig. 9). The relationship of the shear band sets within the damage zones (Figs. 9, 10) suggests that the low-angle R' shears represent an early stage of fault zone nucleation, prior to the formation of R, high-angle R' and P bands, whereas the latter shear bands are related to the more mature stages of fault zone development resulting in complex patterns. Significantly, the shear bands observed within the complex patterns show a constant activity during the evolution of a fault zone. These observations support previous studies of porous sandstones within strike-slip fault zones (e.g. Ahlgren 2001; Katz et al. 2004).

Deformation of cemented, low-porosity limestones (Figs. 12, 13, 14, 15) along fault planes occurs primarily by fracturing and veining with subsequent shearing accompanied by pressure solution and local mass transfer along extensional structures (cf. Crider and Peacock 2004). The subsidiary faults propagated along segmented slip surfaces, often connected by calcite-filled dilational jogs (cf. Segall and Polard 1980; Sibson 1989). The complex structural pattern and textures of calcite veins allow to follow the successive development of fault zones. The presence of various extensional structures, R, R' and R_1' shear fractures and synthetic microfaults or more mature, complex, multilayered fibrous veins parallel to the fault plane in the same sample indicate a subsequent growth of the fault: from a tip damage zone (extension horsetail fractures, wing cracks) through a linking damage zone (dilational jogs) to a wall damage zone (shear fractures, microfaults). Blocky and elongated calcite crystals, occasionally with well-developed faces, and their subperpendicular arrangement with regard to the vein walls indicate that calcite grew in open fractures such as horsetail fractures and wing cracks. In turn, the elongated crystals arranged slightly obliquely to the vein walls may indicate oblique opening of fractures with a shear component and simultaneous infilling with calcite. Both textures display evidence for the further deformation history recorded by deformation lamella within calcite. The elongation and fibrous development of the crystals towards the sense of movement along slip surfaces and the presence of host rock inclusions within crystals arranged subparallel to the vein walls (Figs. 13, 15) confirm the syntectonic growth of calcite during successive opening episodes of veins defined as crack-seal process (Ramsay 1980). Additionally, the formation of bifurcating veins within clusters and their linkage into one or more, wide complex vein(s) suggests control of the deformation pattern by local anisotropy of the host rocks resulting from their heterogeneous texture, e.g. the presence of microfossils and larger grains or change in mineral composition.

Based on studies of strike-slip fault zones and results of laboratory experiments (e.g. Moore and Byerlee 1992; Ahlgren 2001; Katz et al. 2004; Skarbek et al. 2012; Beeler et al. 2013, Wei et al. 2013), we suggest that the slip of the Mieczyn and Gnieździska-Brzeziny faults was accommodated by two modes of slip behaviour: shallow stable sliding or aseismic creep, and stick–slip or seismic. The results of structural observations reveal that both the porous sandstones and the low-porosity limestones display evidence of aseismic and seismic microevents of faulting that has been recorded in rocks within different deformation patterns facilitated most likely by rock fabric and porosity. Thus, we interpret that the early stages of low-angle R' shear band within sandstones can be related to the stable sliding behaviour of the Mieczyn Fault zone. Conversely, cataclasis and shear patterns comprising conjugate R and high-angle R' shears are probably related to the stick–slip behaviour of the fault. By analogy, we interpret that the predomination of R shears within the R–P networks along the Mieczyn Fault damage zone and the development of Riedel shear meshes lacking P shears within limestones from the Gnieździska-Brzeziny Fault damage zone can be also related to the stick–slip behaviour of the studied fault sections (cf. Sibson 1996, 2000). Mineral lineation resulted from the fibrous extensional veins development within dilational jogs occurring along the slip surfaces recording the cyclical opening and infilling by calcite may be related to microearthquakes that were generated by the shallow stable sliding of the fault (cf. Fagereng et al. 2011; Collettini et al. 2011). The syntectonic vein development was

associated with pressure solution of fault plane and host rock, defined as pressure solution creep process (cf. Gratier et al. 2003, 2013). The presence of crack-seal-type extensional veins along faults and shear fractures from different stages of fault development suggests a continuum between the modes of slip during the past activity of the fault (cf. Peng and Gomberg 2010). The evidence of grain-scale dissolution of sandstones and intense dissolution of limestones within damage zones is clear. The dissolution of quartz grains could enhance the slip within sandstones and maintain the fault activity. Conversely, successive episodes of fracture opening and calcite infilling accompanied by pressure solution of limestones probably restrained faulting (cf. Gratier et al. 2011).

Considering fault surface roughness in relationship to slip distance, we have observed decrease in roughness with increasing slip that resulted in smooth fault surfaces. This is consistent with recent detailed studies on this issue within active fault zones (e.g. Sagy et al. 2007; Sagy and Brodsky 2009; Bistacchi et al. 2011). However, we have observed that the degree of smoothing within sandstones does not depend on the scale of faulting, whereas the slip surfaces within limestones are smoother on larger-scale faults in relation to small-scale faults, up to one metre (cf. Power et al. 1988; Candela et al. 2009; Brodsky et al. 2011). The latter show predominantly rough surfaces with high widespread peaks.

Matching the results of field observations and laboratory measurements of selected slip surfaces integrated with structural interpretation of different deformation styles of sandstones and limestones, we suggest that rock fabric and porosity facilitated different mechanical behaviour of rocks resulting in diverse roughness of the slip surfaces. Thus, the slickensides developed in sandstones are distinctly less rough than the slickensides developed in limestones (Figs. 4, 5, 6, 7, 8; Table 2). The 'sandstone' slickenside is smooth due to strong cataclasis and simultaneous cementation by a siliceous matrix along the slip surface. Shear related to slickenside formation had eliminated the high peaks, which could have been preserved in the case of a different mechanism—tension or extension. Single quartz grains or larger rock fragments detached during shearing had a tendency to become inserted in the post-cataclastic surface zone and formed grooves that were parallel to the slip direction. Very smooth slip surfaces could have delimited accumulation of energy on the fault plane and prevent the re-roughing of the slip surface. In turn, the development of slickensides in limestones is relatively more complex due to low rock porosity, their high susceptibility to pressure solution and in consequence the migration of fluids that precipitated calcite within the extensional structures. The presence of structures within a complex internal pattern, typical of various parts of the fault zone, the cross-cutting relationship of structures, the deformational twinning of calcite and pressure solution evidence in one sample (Figs. 13, 14, 15) indicate that the fault planes in the limestones were formed during subsequent multistage evolution with simultaneous infilling of extensional structures with calcite. Hence, the slickenside surfaces in limestones are more rough despite their cryptocrystalline structure, and the multistage process of slow shear favoured the recrystallization of calcite on the slickenside surface. Consequently, even the low anisotropy of the slip surface could result in the accumulation of energy by increasing frictional force on a fault plane that may result in significant increase in roughness.

The presence of fractures and faults reduces the strength of the rocks. Both the observations of fault zones and laboratory experiments (e.g. Morgan 1999; Ben-Zion and Sammis 2003; Lockner et al. 2011) indicate that rocks maintain some residual level of strength after failure. Residual strength is related to the roughness of the fault surfaces—low on smooth surfaces and high on rough surfaces. It determines the friction on the fault surfaces and the susceptibility of rocks to fault development. The application of residual strength analyses in relation to the roughness of the slip surfaces in different lithologies will be investigated in the future study.

Conclusions

The failed rocks within the dextral strike-slip Mieczyn and Gnieździska-Brzeziny fault zones deformed asymmetrically. The intensity of damage is controlled by the geometry of the faults and is clearly higher within the restraining bends than within the releasing bend.

We conclude that fabric and porosity of rocks controlled the failure pattern within damage zones and facilitated diverse roughness of the subsidiary fault surfaces. Both lithologies: sandstones and limestones, accommodated slip by different mechanisms and influenced the fault zone development.

Sandstones display high porosity that enhanced cataclastic shear band formation. The process was accompanied by dissolution of quartz grains within shear deformation bands that resulted in strong cementation and completed the process of porosity reduction across them. Limestones show very low porosity that enhanced the formation of dilatant structures infilled with calcite that precipitated from fluids originated by local rock pressure solution. Extensional type of failure of limestones is independent of their position within the extensional or contractional sectors of the non-planar fault.

The complex structural pattern of damage zones within sandstones and limestones shows evidence of multiple episodes

of slip and continuous mixed mode of fault slip behaviour. Different deformational patterns recorded by the rocks give hints on the crucial role of the paleoseismicity in shallow-genearated damage of rocks within strike-slip fault zones.

Therefore, knowledge of the structural pattern of damage zones and the roughness of slip surfaces can be applied in interpretations of seismic–aseismic behaviour of faults. The proposed methodology can be used also in the analysis of seismically active fault zones.

Acknowledgments The study was supported by Grant No. 2011/03/B/ST10/06341 of the National Science Centre, Poland 'Role of strike-slip faulting during the inversion of the south-western part of the Holy Cross segment of the Polish Basin'. We thank Lorenzo Bonini, anonymous reviewer and Soumyajit Mukherjee for constructive comments that helped improve the manuscript.

References

Ahlgren SG (2001) The nucleation and evolution of Riedel shear zones as deformation bands in porous sandstone. J Struct Geol 23:1203–1214. doi:10.1016/S0191-8141(00)00183-8

Aydin A (1978) Small faults formed as deformation bands in sandstone. Pure appl Geophys 116:913–930. doi:10.1007/BF00876546

Aydin A, Johnson AM (1983) Analysis of faulting in porous sandstones. J Struct Geol 5:19–31. doi:10.1016/0191-8141(83)90004-4

Aydin A, Borja RI, Eichhubl P (2006) Geological and mathematical framework for failure modes in granular rock. J Struct Geol 28:83–98. doi:10.1016/j.jsg.2005.07.008

Beeler NM, Thomas A, Bürgmann R, Shelly D (2013) Inferring fault rheology from low-frequency earthquakes on the San Andreas. J Geophys Res Solid Earth 118:5976–5990. doi:10.1002/2013JB010118

Ben-Zion Y, Sammis CC (2003) Characterization of fault zones. Pure appl Geophys 160:677–715

Ben-Zion Y, Shi Z (2005) Dynamic rupture on a material interface with spontaneous generation of plastic strain in the bulk. Earth Planet Sci Lett 236:486–496. doi:10.1016/j.epsl.2005.03.025

Billi A, Salvini F, Storti F (2003) The damage zone-fault core transition in carbonate rocks: implications for fault growth structure and permeability. J Struct Geol 25:1779–1794. doi:10.1016/S0191-8141(03)00037-3

Bistacchi A, Griffith WA, Smith SAF, Di Toro G, Jones R, Nielsen S (2011) Fault roughness at seismogenic depths from LIDAR and photogrammetric analysis. Pure appl Geophys 168:2345–2363. doi:10.1007/s00024-011-0301-7

Blenkinsop TG (2008) Relationships between faults extension fractures and veins and stress. J Struct Geol 30:622–632. doi:10.1016/j.jsg.2008.01.008

Brodsky EE, Gilchrist JJ, Sagy A, Collettini C (2011) Faults smooth gradually as a function of slip. Earth Planet Sci Lett 302:185–193. doi:10.1016/j.epsl.2010.12.01

Bullock RJ, De Paola N, Holdsworth RE, Trabucho-Alexandre J (2014) Lithological controls on the deformation mechanisms operating within carbonate-hosted faults during the seismic cycle. J Struct Geol 58:22–42. doi:10.1016/j.jsg.2013.10.00

Caine JS, Forster CB (1999) Fault zone architecture and fluid flow; insights from field data and numerical modeling. In: Haneberg WC, Mozley PS, Moore JC, Goodwin LB (eds) Faults and subsurface fluid flow in the shallow crust. AGU geophysical monograph, vol 113. American Gephysical Union, Washington, D.C., pp 101–127

Caine JS, Evans JP, Forster CB (1996) Fault zone architecture and permeability structure. Geology 24:1025–1028

Caine JS, Bruhn RL, Forster CB (2010) Internal structure fault rocks and inferences regarding deformation fluid flow and mineralization in the seismogenic stillwater normal fault, Dixie Valley Nevada. J Struct Geol 32:1576–1589. doi:10.1016/j.jsg.2010.03.00

Candela T, Renard F, Bouchon M, Marsan D, Schmittbuhl J, Voisin C (2009) Characterization of fault roughness at various scales: implications of three-dimensional high resolution topography measurements. Pure appl Geophys 166:1817–1851. doi:10.1007/s00024-009-0521-2

Chester FM, Logan JM (1986) Implications for mechanical-properties of brittle faults from observations of the Punchbowl fault zone, California. Pure appl Geophys 124:79–106. doi:10.1007/BF0087572

Cieśla E, Lindner L (1990) Geological Map of Poland. Końskie sheet. Wydawnictwa Geologiczne, Warszawa, scale 1:50,000

Colletttini C, Niemeijer A, Viti C, Smith AF, Marone C (2011) Fault structure, frictional properties and mixed-mode fault slip behavior. Earth Planet Sci Lett 311:316–327

Crider JG, Peacock DCP (2004) Initiation of brittle faults in the upper crust: a review of field observations. J Struct Geol 26:691–707. doi:10.1016/j.jsg.2003.07.007

Cruikshank KM, Zhao G, Johnson AM (1991) Analysis of minor fractures associated with joints and faulted joints. J Struct Geol 13:865–886. doi:10.1016/0191-8141(91)90083-U

Czarnocki J (1938) Carte géologique générale de la Pologne scale 1:100,000 feuille 4 Kielce. Edition du Service Géologique de Pologne

Czarnocki J (1948) Przewodnik 20 Zjazdu Polskiego Towarzystwa Geologicznego w Górach Świętokrzyskich w r. 1947. Rocz Pol Towarz Geol 17:237–299

Czarnocki J (1950) Geology of the Łysa Góra Region (Święty Krzyż Mountains) in connection with the problem of iron ores at Rudki. Prace Państwowego Instytutu Geologicznego 1:1–404 **(In Polish with English summary)**

Czarnocki J (1961) Materiały do przeglądowej mapy geologicznej Polski. Region Świętokrzyski. Arkusz Kielce. Wyd. B zaktualizowane. Wydawnictwa Geologiczne, Warszawa, scale 1:100,000

Dadlez R (1997) Epicontinental basins in Poland: Devonian to Cretaceous-relationship between the crystalline basement and sedimentary infill. Geol Q 41:419–432

Dadlez R (2003) Mesozoic thickness pattern in the Mid-Polish Trough. Geol Q 47:223–240

Dadlez R, Narkiewicz M, Stephenson RA, Visser MTM, Van Wees J-D (1995) Tectonic evolution of the Mid-Polish Trough: modelling implications and significance for central European geology. Tectonophysics 252:179–195

Dadlez R, Jóźwiak W, Młynarski S (1997) Subsidence and inversion in the western part of Polish basin—data from seismic velocities. Geol Q 41:197–208

DIN EN ISO 4287: 2010-07. Geometrical Product Specifications (GPS)—Surface texture: Profile method—Terms, definitions and surface texture parameters (ISO, Geneva 2010)

Doblas M (1998) Slickenside kinematic indicators. Tectonophysics 295(1–2):187–197

Dor O, Chester JS, Ben-Zion Y, Brune JN, Rockwell TK (2009) Characterization of damage in sandstones along the Mojave section of the San Andreas Fault: implications for the shallow extent of damage generation. Pure appl Geophys 166:1747–1773. doi:10.1007/s00024-009-0516-z

Dunham RJ (1962) Classification of carbonate rocks according to depositional texture. In: Hamm WE (ed) Classification of carbonate rocks. A SYMPOSIUM. American Association of Petroleum Geologists, pp 108–121

EUR 15178 EN (1993) The Development of Methods for the Characterization of Roughness in three dimensions (European Commission, Brussels 1993)

Fagereng Å, Remitti F, Sibson RH (2011) Incrementally developed slickenfibers—geological record of repeating low stress-drop seismic events? Tectonophysics 510:381–386. doi:10.1016/j.tecto.2011.08.015

Faulkner DR, Jackson CAL, Lunn RJ, Schlische RW, Shipton ZK, Wibberley CAJ, Withjack MO (2010) A review of recent developments concerning the structure mechanics and fluid flow properties of fault zones. J Struct Geol 32:1557–1575. doi:10.1016/j.jsg.2010.06.009

Filonowicz P (1967) Geological Map of Poland, Morawica sheet. Wydawnictwa Geologiczne, scale 1:50,000

Filonowicz P (1973) Geological Map of Poland, Kielce sheet. Wydawnictwa Geologiczne,Warszawa, scale 1:50,000

Filonowicz P, Lindner L (1986) Geological Map of Poland, Piekoszów sheet. Wydawnictwa Geologiczne,Warszawa, scale 1:50,000

Finzi Y, Hearn EH, Ben-Zion Y, Lyakhovsky V (2009) Structural properties and deformation patterns of evolving strike-slip faults: numerical simulations incorporating damage rheology. Pure appl Geophys 166:1537–1573. doi:10.1007/s00024-009-0522-1

Fossen H, Hesthammer J (1997) Geometric analysis and scaling relations of deformation bands in porous sandstone. J Struct Geol 19:1479–1493

Fossen H, Schultz RA, Shipton ZK, Mair K (2007) Deformation bands in sandstone: a review. J Geol Soc Lond 164:755–769. doi:10.1144/0016-76492006-036

Freund R (1974) Kinematics of transform and transcurrent faults. Tectonophysics 21:93–134. doi:10.1016/0040-1951(74)90064-X10.1016/0040-1951(74)90064-X

Garfunkel Z, Zak I, Freund R (1981) Active faulting in the Dead Sea rift. Tectonophysics 80:1–26. doi:10.1016/0040-1951(81)90139-6

Golonka J, Oszczypko N, Ślączka A (2000) Late Carboniferous-Neogene geodynamic evolution and palaeogeography of the circum–Carpathian region and adjacent areas. Ann Soc Geol Pol 70:107–136

Gratier JP, Favreau P, Renard F (2003) Modeling fluid transfer along California faults when integrating pressure solution crack sealing and compaction processes. J Geophys Res 108(B2):28–52

Gratier JP, Richard J, Renard F, Mittempergher S, Doan ML, Di Toro G, Hadizadeh J, Boullier AM (2011) Aseismic sliding of active faults by pressure solution creep: evidence from the San Andreas Fault Observatory at depth. Geology 39:1131–1134. doi:10.1130/G32073.1

Gratier JP, Dysthe D, Renard F (2013) The role of pressure solution creep in the ductility of the Earth's upper crust. Adv Geophys 54:47–179

Grzybowski K, Kutek J (1967) Geological Map of Poland, Lubień sheet. Wydawnictwa Geologiczne, Warszawa, scale 1:50,000

Guterch A, Grad M, Keller G R, Posgay K, Vosar J, Spicak A, Brueckel E, Haynal Z, Thybo H, Selvi O (2000) The Celebration 2000 Seismic Experiment. Joint Meeting of EURO-PROBE (TESZ) and PACE Projects. Zakopane/Holy Cross Mountains, Poland. Abstracts volume, 29–32

Hakenberg M (1973) Geological Map of Poland, Chęciny sheet. Wydawnictwa Geologiczne, Warszawa, scale 1:50,000

Harding TP (1985) Seismic characteristics and identification of negative flower structures positive flower structures and positive structural inversion. Am Assoc Pet Geol B 69:582–600

Heimann A, Ron H (1987) Young faults in the Hula Pull-Apart Basin, central Dead Sea Transform. Tectonophysics 141:117–124. doi:10.1016/0040-1951(87)90179-X

Hesthammer J, Fossen H (2001) Structural core analysis from the Gullfaks area northern North Sea. Mar Pet Geol 18:411–439. doi:10.1016/S0264-8172(00)00068-4

Janiec J (1991) Geological Map of Poland. Żarnów sheet. Wydawnictwa Geologiczne, Warszawa, scale 1:50,000

Johansen TES, Fossen H, Kluge R (2005) The impact of syn-faulting porosity reduction on damage zone architecture in porous sandstone: an outcrop example from the Moab Fault Utah. J Struct Geol 27:1469–1485. doi:10.1016/j.jsg.2005.01.014

Jurkiewicz I (1961) Materiały do Przeglądowej mapy geologicznej Polski. Region Świętokrzyski, arkusz Przedbórz. Wydanie B zaktualizowane, skala 1:100,000. Wydawnictwa Geologiczne, Warszawa

Jurkiewicz I (1965) Geological Map of Poland, Czermno sheet. Wydawnictwa Geologiczne, Warszawa, scale 1:50,000

Jurkiewicz I (1967) Geological Map of Poland, Radoszyce sheet. Wydawnictwa Geologiczne, Warszawa, scale 1:50,000

Katz Y, Weinberger R, Aydin A (2004) Geometry and kinematic evolution of Riedel shear structures, Capitol Reef National Park, Utah. J Struct Geol 26:491–550. doi:10.1016/j.jsg.2003.08.003

Knipe RJ, Fisher QJ, Jones G, Clennell MR, Farmer AB, Harrison A, Kidd B, Mcallister E, Porter JR, White EA (1997) Fault seal analysis: successful methodologies application and future directions. Nor Pet Soc Spec Publ 7:15–38. doi:10.1016/S0928-8937(97)80004-5

Konon A (2006) Buckle folding in the Kielce Unit, Holy Cross Mountains, central Poland. Acta Geol Pol 56:375–405

Konon A (2007) Strike-slip faulting in the Kielce Unit, Holy Cross Mountains, central Poland. Acta Geol Pol 57:415–441

Konon A (2015) Przejawy przesuwczości w obrębie południowo-zachodniego obrzeżenia permsko-mezozoicznego Gór Świętokrzyskich. LXXXIV Zjazd Naukowy Polskiego Towarzystwa Geologicznego, Chęciny, 9-11 września 2015, Ekstensja i inwersja powaryscyjskich basenów sedymentacyjnych

Konon A, Ostrowski S, Rybak-Ostrowska B, Ludwiniak M, Śmigielski M, Wyglądała M, Uroda J, Kowalczyk S, Mieszkowski R, Kłopotowska A (2016) Mnin restraining stepover–evidence of significant Cretaceous–Cenozoic dextral strike-slip faulting along the Teisseyre–Tornquist Zone? Acta Geol Pol. doi:10.1515/agp-2016-0022

Konon A, Mastella L (2001) Structural evolution of the Gnieździska Syncline—regional implications for the SW Mesozoic Margin of the Holy Cross Mountains (Central Poland). Ann Soc Geol Pol 71:189–199

Krajewski R. (1961) Materiały do Przeglądowej mapy geologicznej Polski. Region Świętokrzyski, arkusz Końskie. Wydanie B zaktualizowane, skala 1:100,000. Wydawnictwa Geologiczne Warszawa

Krauze A (2015) Petrophysical analysis of the Gnieździska-Brzeziny fault zone in the region of Miedzianka (Holy Cross Mountains). In Polish. Master thesis, University of Warsaw

Krzywiec P (2000) O mechanizmach inwersji bruzdy środkowopolskiej—wyniki interpretacji danych sejsmicznych. Biuletyn Państwowego Instytutu Geologicznego 393:135–166

Krzywiec P (2002) Mid–Polish Trough inversion—seismic examples, main mechanism, and its relationship to the Alpine–Carpathian collision, EGU Stephan Mueller Special Publication series 1

Kutek J (2001) The Polish Permo-Mesozoic Rift Basin. In: Ziegler PA et al (eds) Peri-Tethyan Rift/Wrench Basins and Passive Margins. Peri-Tethys memoir 6. Mem Mus Natn Hist Nat 186: 213–236

Kutek J, Głazek J (1972) The Holy Cross area, Central Poland, in the Alpine cycle. Acta Geol Pol 22:603–653

Kwapisz B (1983) Geological Map of Poland, Przedbórz sheet. Wydawnictwa Geologiczne, Warszawa, scale 1:50,000

Lockner DA, Morrow C, Moore D, Hickman S (2011) Low strength of deep San Andreas fault gouge from SAFOD core. Nature 472:82–85. doi:10.1038/nature09927

Mastella L, Konon A (2002) Non-planar strike-slip Gnieździska-Brzeziny fault (SW Mesozoic margin of the Holy Cross Mountains central Poland). Acta Geol Pol 52:471–480

Matyja BA (2009) Development of the Mid-Polish Trough versus Late Jurassic evolution in the Carpathian Foredeep area. Geol Q 53:49–62

Mazur S, Krzywiec P, Scheck-Wenderoth M (2005) Different modes of Late Cretaceous-Ealy Tertiary inversion in the North German and Polish Basin. Int J Earth Sci 94:782–798

Means WD (1987) A newly recognised type of slickenside striation. J Struct Geol 9:585–590

Micarelli L, Benedicto A, Wibberley C (2006) Structural evolution and permeability of normal fault zones in highly porous carbonate rocks. J Struct Geol 28:1214–1227. doi:10.1016/j.jsg.2006.03.036

Michie EAH, Haines TJ, Healy D, Neilson JE, Timms NE, Wibberley CAJ (2014) Influence of carbonate facies on fault zone architecture. J Struct Geol 65:82–99. doi:10.1016/j.jsg.2014.04.007

Moore DE, Byerlee J (1992) Relationships between sliding behavior and internal geometry of laboratory fault zones and some creeping and locked strike-slip faults of California. Tectonophysics 211:305–316. doi:10.1016/0040-1951(92)90067-G

Morgan JK (1999) Numerical simulations of granular shear zones using the distinct element method: 2. Effects of particle size distribution and interparticle friction on mechanical behaviour. J Geophys Res Solid Earth 104(B2):2721–2732. doi:10.1029/1998JB900055

Mukherjee S (2010) Structures in Meso- and Micro-scales in the Sutlej section of the Higher Himalayan Shear Zone, Indian Himalaya. e-Terra 7:1–27

Mukherjee S (2013a) Higher Himalaya in the Bhagirathi section (NW Himalaya, India): its structures, backthrusts and extrusion mechanism by both channel flow and critical taper mechanisms. Int J Earth Sci 102:1851–1870

Mukherjee S (2013b) Deformation microstructures in rocks. Springer, Berlin

Mukherjee S (2015) Atlas of structural geology. Elsevier, Amsterdam

Mukherjee S, Koyi HA (2010) Higher Himalayan Shear Zone, Sutlej Section- structural geology and extrusion mechanism by various combinations of simple shear, pure shear and channel flow in shifting modes. Int J Earth Sci 99:1267–1303

Nicol A, Childs C, Walsh JJ, Schafer KW (2013) A geometric model for the formation of deformation band clusters. J Struct Geol 55:21–33. doi:10.1016/j.jsg.2013.07.004

Peng Z, Gomberg J (2010) An integrated perspective of the continuum between earthquakes and slow-slip phenomena. Nat Geosci 3:599–607. doi:10.1038/ngeo940

Petit JP (1987) Criteria for the sense of movement on fault surfaces in brittle rocks. J Struct Geol 9:597–608

Pettijohn FJ, Potter PE, Siever R (1972) Sand and sandstones. Springer, New York

Power WL, Tullis TE, Weeks JD (1988) Roughness and wear during brittle faulting. J Geophys Res 93:268–278

Ramsay JG (1980) The crack-seal mechanism of rock deformation. Nature 284:135–139. doi:10.1038/284135a0

Renard F, Voisin C, Marsan D, Schmittbuhl J (2006) High resolution 3D laser scanner measurements of a strike-slip fault quantify its morphological anisotropy at all scales. Geophys Res Lett 33:L04305. doi:10.1029/2005GL025038

Riedel W (1929) Zur Mechanik geologischer Brucherscheinumgen. Zentralblatt für Mineralogie, Geologie und Paläontologie, Abt B

Różycki SZ (1961) Materiały do Przeglądowej mapy geologicznej Polski. Region Świętokrzyski, arkusz Włoszczowa. Wydanie B zaktualizowane, skala 1:100,000. Wydawnictwa Geologiczne, Warszawa

Sagy A, Brodsky EE (2009) Geometric and theological asperities in an exposed fault zone. J Geophys Res Solid Earth 114:B02301. doi:10.1029/2008JB005701

Sagy A, Brodsky EE, Axen GJ (2007) Evolution of fault-surface roughness with slip. Geology 35:283–286. doi:10.1130/G23235A.1

Scheck M, Lamarche J (2005) Crustal memory and basin evolution in the Central European Basin System—new insights from a 3D structural model. Tectonophysics 397:143–165

Scheck M, Bayer U, Otto V, Lamarche J, Banka D, Pharaoh T (2002) The Elbe Fault System in North Central Europe—a basement controlled zone of crustal weakness. Tectonophysics 360:281–299

Segall P, Polard DD (1980) Mechanics of discontinuous faults. J Geophys Res 85:4337–4350

Senkowicz E (1958) Geological Map of Poland, Pińczów sheet. Wydawnictwa Geologiczne, Warszawa, scale 1:50,000

Shipton ZK, Cowie PA (2003) A conceptual model for the origin of fault damage zone structures in high-porosity sandstone. J Struct Geol 25:1343–1345. doi:10.1016/S0191-8141(02)00037-8

Sibson RH (1977) Fault rocks and fault mechanisms. J Geol Soc Lond 133:191–213. doi:10.1144/gsjgs.133.3.0191

Sibson RH (1989) Earthquake faulting as a structural process. J Struct Geol 11:1–14. doi:10.1016/0191-8141(89)90032-1

Sibson RH (1996) Structural permeability of fluid-driven fault-fracture meshes. J Struct Geol 18:1031–1042. doi:10.1016/0191-8141(96)00032-6

Sibson RH (2000) Fluid involvement in normal faulting. J Geodyn 29:469–499. doi:10.1016/S0264-3707(99)00042-3

Skarbek RM, Rempel AW, Schmidt DA (2012) Geologic heterogeneity can produce aseismic slip transients. Geophys Res Lett 39:L21306. doi:10.1029/2012GL053762

Sylvester AG (1988) Strike-slip faults. Bull Geol Soc Am 100:1666–1703. doi:10.1130/0016-7606(1988)100<1666:SSF>2.3.CO;2

Szajn J (1977) Geological Map of Poland, Nagłowice sheet. Wydawnictwa Geologiczne, Warszawa, scale 1:50,000

Szajn J (1980) Geological Map of Poland, Włoszczowa sheet. Wydawnictwa Geologiczne, Warszawa, scale 1:50,000

Szajn J (1983) Geological Map of Poland, Oleszno sheet. Wydawnictwa Geologiczne, Warszawa, scale 1:50,000

Underhill JR, Woodcock NH (1987) Faulting mechanisms in high-porosity sandstones; new red sandstone, Arran, Scotland. Geol Soc Lond Spec Publ 29:91–105

Wei M, Kaneko Y, Liu Y, McGuire JJ (2013) Episodic fault creep events in California controlled by shallow frictional heterogeneity. Nat Geosci 6:566–570. doi:10.1038/ngeo1835

Wilcox RE, Harding TP, Seely DR (1973) Basic wrench tectonics. AAPG Bull 57:74–96

Woodcock NH, Fischer M (1986) Strike-slip duplexes. J Struct Geol 8:725–735. doi:10.1016/0191-8141(86)90021-0

Woodcock NH, Schubert C (1994) Continental strike-slip tectonics. In: Hancock PL (ed) Continental deformation. Pergamon Press, New York, pp 251–263

Ziegler PA (1982) Geological atlas of Western and Central Europe. Elsevier, Amsterdam, pp 1–130

Ziegler PA (1987) Late Cretaceous and Cenozoic intra-plate compressional deformations in the Alpine foreland—a geodynamic model. Tectonophysics 137:389–420

Ziegler PA (1990a) Collision related intra-plate compression deformations in Western and Central Europe. J Geodyn 11:357–388

Ziegler PA (1990b) Geological Atlas of Western and Central Europe. In: Shell Internationale Petroleum Mij. BV and Geological Society of London, 2nd edn, pp 1–239